Precambrian Research 313 (2018) 31–50

Contents lists available at ScienceDirect

Precambrian Research

journal homepage: www.elsevier.com/locate/precamres

Isotopic insight into the Proterozoic crustal evolution of the Rudall Province, Western Australia

N.J. Gardiner[a,b,c,*], D.W. Maidment[d], C.L. Kirkland[a,b,c], S. Bodorkos[e], R.H. Smithies[d], H. Jeon[f,1]

[a] Centre for Exploration Targeting – Curtin Node, School of Earth and Planetary Sciences, Curtin University, Perth, WA 6102, Australia
[b] The Institute for Geoscience Research (TIGeR), School of Earth and Planetary Sciences, Curtin University, GPO Box U1987, Perth, WA 6845, Australia
[c] Australian Research Council Centre of Excellence for Core to Crust Fluid Systems, Australia
[d] Geological Survey of Western Australia, Department of Mines, Industry Regulation and Safety, 100 Plain Street, East Perth, WA 6004, Australia
[e] Geoscience Australia, GPO 378, Canberra, ACT 2601, Australia
[f] Centre for Microscopy, Characterisation and Analysis, University of Western Australia, Perth, WA 6009, Australia

ARTICLE INFO

Keywords:
West Australian Craton
North Australian Craton
Pilbara
Zircon Hf O isotopes
Proterozoic belt

ABSTRACT

The Proterozoic assembly of Australia involved the convergence of three main Archean cratonic entities: the North, West and South Australian Cratons, and is recorded in the Proterozoic orogenic belts surrounding these continental nuclei. The Rudall Province of northern Western Australia is the sole exposure of a Paleo- to Mesoproterozoic orogen lying between the North and West Australian Cratons, and may record the effects of their amalgamation. We present new zircon O, U–Pb and Lu–Hf isotope data from magmatic rocks across the Rudall Province, to which we add existing isotope data to yield a crustal evolution overview. Hf evolution trends for the ca. 1804–1762 Ma Kalkan Supersuite, the ca. 1589–1549 Ma Krackatinny Supersuite and the ca. 1310–1286 Ma Camel Suite, indicate a significant input of Archean East Pilbara Basement material, albeit as a mix with more juvenile material, including a possible ca. 1900 Ma component. Zircon $\delta^{18}O$ data suggest a contribution from supracrustal material into the magmatic source of the Kalkan Supersuite, which may have been emplaced in an extensional setting. In contrast, the Krackatinny Supersuite and Camel Suite have mantle-like $\delta^{18}O$ which may reflect partial melting of deeper Archean sources. Geochemical data for the Krackatinny Supersuite shows geochemical trends implying that melting of thickened mafic crust progressed from deeper to shallower levels, possibly in a rift setting. Camel Suite K-rich leucogranites may also have been emplaced in an extensional setting towards the end of high-P metamorphism. All terranes of the Rudall Province are para-autochthonous with respect to the Pilbara Craton, with no requirement for arc-related magmatism. We outline two potential scenarios for the Paleo- to Mesoproterozoic geodynamic evolution of the Rudall Province: an early cratonic amalgamation between the West and North Australian Cratons ca. 1680 Ma followed by Mesoproterozoic intraplate events; or a later assembly ca. 1377–1275 Ma. We lean towards this later amalgamation scenario.

1. Introduction

Proterozoic rocks situated along the periphery of many Archean cratonic nuclei chart the reorganization and amalgamation of crust into larger entities. The Proterozoic assembly of Australia involved the convergence and stabilization of three main cratonic entities: the North Australian Craton, the West Australian Craton and the South Australian Craton (Betts and Giles, 2006; Cawood and Korsch, 2008; Huston et al., 2012; Myers et al., 1996). This assembly of proto-Australia is recorded in the Proterozoic orogenic belts surrounding these Archean continental nuclei, though the evidence is often obscured by younger crustal reworking and/or limited exposure.

The West Australian Craton is itself a composite entity comprising the Pilbara and Yilgarn Cratons, which were assembled into the West Australian Craton along the Capricorn Orogen during the late Paleoproterozoic (ca. 2000–1950 Ma) Glenburgh Orogeny (Johnson et al., 2013; Occhipinti et al., 2004). The North Australian Craton (Myers et al., 1996; Plumb, 1979) consists of an assemblage of Neoarchean to Paleoproterozoic terranes in northern Australia that are overlain by a series of late Paleoproterozoic to Neoproterozoic basins. There are differences between interpretations regarding the crustal elements that comprise the southern margins of the North Australian

* Corresponding author at: Centre for Exploration Targeting – Curtin Node, School of Earth and Planetary Sciences, Curtin University, Perth, WA 6102, Australia.
E-mail address: nicholas.gardiner@curtin.edu.au (N.J. Gardiner).
[1] Present address: Swedish Museum of Natural History, Box 50007, 10405 Stockholm, Sweden.

https://doi.org/10.1016/j.precamres.2018.05.003
Received 1 November 2017; Received in revised form 29 March 2018; Accepted 3 May 2018
Available online 04 May 2018

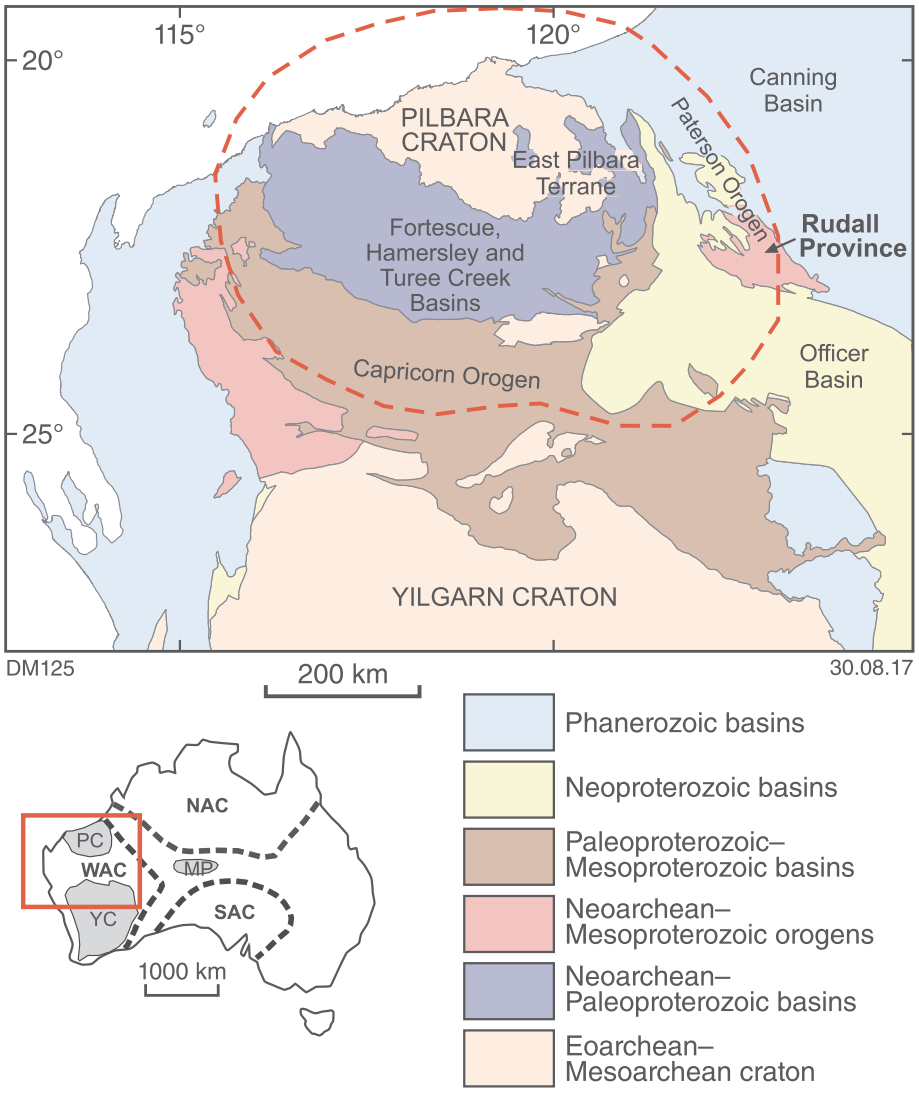

Fig. 1. Simplified geological map indicating the location of the Rudall Province relative to other Proterozoic orogens and Archean cratons within Western Australia (modified after Sheppard et al., 2010). Red dashed line indicates the approximate subsurface extent of the Pilbara Craton, which is interpreted to at least partially underlie the Rudall Province. Inset map shows the location of the main map, and the WAC (West Australian Craton), which itself comprises the Pilbara Craton (PC) and the Yilgarn Craton (YC), in the context of other tectonic entities. Abbreviations: CG – Capricorn Group, GC – Gawler Craton, GT – Glenburgh Terrane, KC – Kimberley Craton, LRF – Lyons River Fault, NAC – North Australian Craton, SAC – South Australian Craton. (For interpretation of the references to colour in this figure legend, the reader is referred to the web version of this article.)

Craton (Bagas et al., 2014; Betts et al., 2016; Cawood and Korsch, 2008), but in this paper we consider the craton to incorporate all of the outcropping Arunta Orogen. The southwestern extent of the North Australian Craton is unclear as it is entirely covered by the Phanerozoic Canning Basin. It is possible that much of the crust beneath the Canning Basin forms part of the North Australian Craton, but the character of deep crustal seismic data raises the possibility that the Canning Basin may in part be underlain by an intervening crustal block that is distinct from both the North and West Australian Cratons (Frogtech Geoscience, 2017; Maidment and Zhan, 2016).

The Rudall Province of northern Western Australia (Fig. 1) is the sole exposure of a Paleo- to Mesoproterozoic orogen between the West and North Australian Cratons, and may therefore record key features related to the effects of Proterozoic plate margin processes during their assembly (Bagas, 2004; Betts et al., 2016; Betts and Giles, 2006; Smithies and Bagas, 1997). In this, the Rudall Province may represent the only direct evidence of the final assembly of these cratons, as the junction further south between the West Australian Craton and the South Australian Craton comprises the remnants of the nascent ca. 1900 Ma Mirning Ocean, which was never fully consumed (Kirkland et al., 2017). The rocks within the Rudall Province reflect, in part, the intensely modified margin of the Pilbara Craton, part of the West Australian Craton, which is overlain by Paleoproterozoic supracrustal rocks, and intruded by Paleo- to Mesoproterozoic plutons (Kirkland et al., 2013b).

The amalgamation of the West and North Australian cratons has previously been interpreted to be coeval with ca. 1800–1760 Ma felsic magmatism and high-pressure metamorphism assigned to the Yapungku Orogeny (Bagas, 2004; Hickman and Bagas, 1999), and this timing has subsequently been incorporated into most models of the Proterozoic assembly of Australia (e.g., Betts et al., 2016; Betts and Giles, 2006; Cawood and Korsch, 2008; Huston et al., 2012). Recent work, however, has raised the possibility that the high-pressure metamorphism considered to be associated with the amalgamation of the cratons took place later than previously thought, possibly as late as ca. 1.3 Ga (Anderson, 2015; Maidment, 2017).

Due to the lack of exposure and geological complexity of this region, isotope geochemistry is a valuable tool with which to resolve key geological questions such as the location of terrane boundaries, the nature of magmatism, and the basement architecture. In this study we present new zircon O, U–Pb and Lu–Hf isotope data from the three terranes comprising the Rudall Province. We then synthesize all available zircon U–Pb, Lu–Hf, O and whole-rock Sm–Nd data from the Rudall Province to yield a crustal evolution overview of this key region, and use it to explore the assembly of the North Australian Craton and the West Australian Craton.

2. Regional geology

The Rudall Province, ~100 km east of the Paleo- to Neoarchean

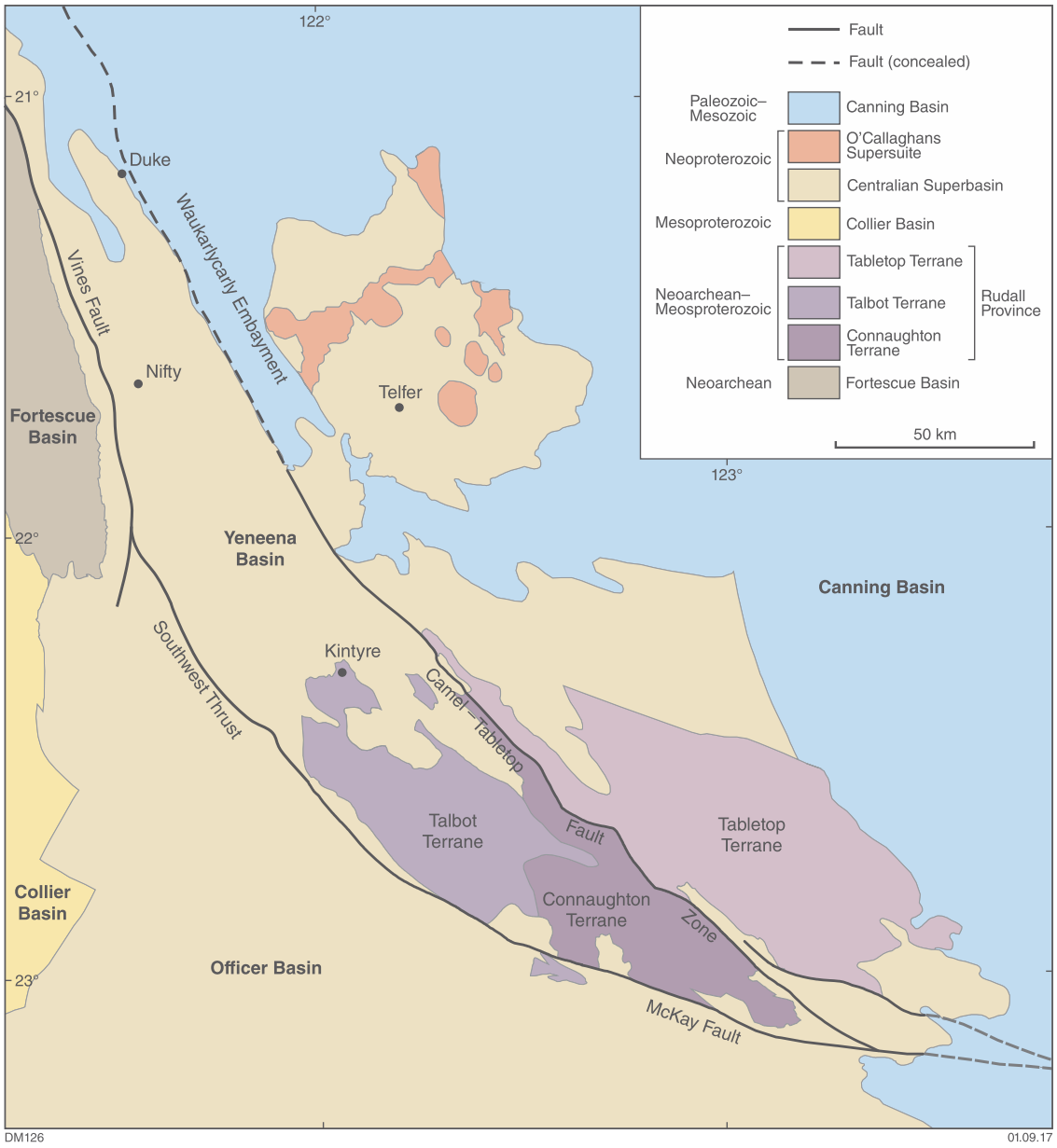

Fig. 2. Geological terrane map of the Rudall Province, and surrounding basins. Major deposits in the area are the Telfer (Au–Cu), Nifty (Cu) and Kintyre (U). Also shown is the location of the Duke prospect.

Pilbara Craton, is situated near the northeastern edge of the West Australian Craton, and forms part of the Paterson Orogen (Fig. 1). It comprises a northwesterly trending belt of multiply deformed and metamorphosed Paleo- to Mesoproterozoic supracrustal and igneous rocks which is unconformably overlain by Neoproterozoic sedimentary rocks of the Yeneena and Officer Basins, and Paleozoic to Mesozoic sedimentary rocks of the Canning Basin (Fig. 2). These sedimentary basins also separate the Rudall Province from the Mesoproterozoic Musgrave Province in Central Australia (Fig. 1), which records Meso- to Neoproterozoic tectonothermal events similar to those in the Paterson Orogen. Both the Rudall and Musgrave Provinces, and deformed Neoproterozoic sedimentary units, have been interpreted as part of the 2000 km-long Paterson–Petermann Orogenic belt (Bagas, 2004). However, the link between the two provinces remains unclear.

The Rudall Province contains supracrustal rocks of Paleoproterozoic to possible Neoarchean age, which have been intruded by voluminous Paleoproterozoic to Mesoproterozoic granitic rocks and overprinted by multiple episodes of metamorphism and deformation. The age and number of metasedimentary successions in the province is currently relatively poorly constrained, with maximum depositional ages obtained from dating of detrital zircons ranging between ca. 2833 and 1791 Ma (GSWA, 2016; Maidment, 2017). These rocks have been intruded by three main felsic magmatic suites: the 1804–1762 Ma Kalkan Supersuite; the 1589–1549 Ma Krackatinny Supersuite, and the 1310–1286 Ma Camel Suite (Bagas, 2004; Budd et al., 2002; Maidment, 2017).

The highest-grade metamorphism recorded in the Rudall Province attained peak pressures of 0.8–1.2 GPa, which has been interpreted to reflect a continental collision (Bagas, 2004; Hickman and Bagas, 1999; Smithies and Bagas, 1997). This metamorphism has previously been inferred to be broadly coeval with the emplacement of voluminous granitic rocks of the Kalkan Supersuite during the Yapungku Orogeny at ca. 1800–1760 Ma. The inferred continental collision at this time has been suggested to reflect the collision of the West and North Australian cratons and has formed a pinning point in most models of the Proterozoic assembly of Australia (Betts and Giles, 2006; Cawood and Korsch,

2008; Huston et al., 2012). Recent studies, however, have suggested that the high-pressure metamorphism interpreted to record collision may in fact significantly post-date granite emplacement, on the basis of U–Pb dates for metamorphic zircon and monazite ranging between ca. 1380 and 1275 Ma (Anderson, 2015; Maidment, 2017). This metamorphic event has not been previously named, but is here termed the Parnngurr Orogeny after a settlement central to the area where this metamorphism has been defined. The term Yapungku Orogeny is here defined to refer to tectonism associated with the emplacement of the 1804–1762 Ma Kalkan Supersuite.

A Mesoproterozoic timing for the high-pressure metamorphism in turn raises questions about the timing of terrane amalgamation, assuming that this metamorphism does in fact record the effects of a collision rather than intraplate reworking. A Mesoproterozoic age for collision would also require re-assessment of the setting of other Paleo- to Mesoproterozoic tectonothermal events recorded within the Rudall Province.

Significant Neoproterozoic deformation during the ca. 800–630 Ma Miles Orogeny and the ca. 550 Ma Paterson Orogeny affected both the Rudall Province and the unconformably overlying Yeneena Basin (Bagas, 2004). The Miles Orogeny produced northwest-trending folds and thrusts with similar orientation to structures generated during the Yapungku Orogeny, but at significantly lower grade (typically greenschist facies). The Paterson Orogeny is interpreted to have involved transpression and dextral strike-slip movement on major northwest-trending faults (Bagas, 2004).

2.1. Terranes of the Rudall Province

The Rudall Province has been subdivided into three crustal blocks; the Talbot, Connaughton, and Tabletop terranes (Bagas and Smithies, 1998) (Fig. 3). These terranes are bounded by major faults, which are interpreted to have been active during Paleo- to Mesoproterozoic tectonism and Neoproterozoic reworking (Bagas, 2004). Despite some apparent differences between the geological histories of these terranes, they appear to represent para-autochthonous blocks, based on the ages and Lu–Hf isotopic character of zircons from igneous and metasedimentary units (Kirkland et al., 2013b; Maidment, 2017). A geological map of the Rudall Province showing the locations of samples discussed in the present study is presented in Fig. 4.

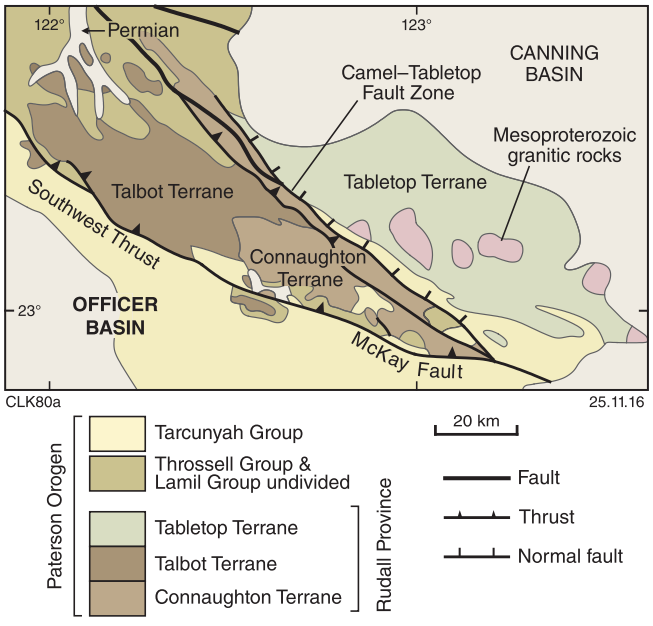

Fig. 3. Simplified geological map of the Rudall Province, indicating the main lithotectonic zones and surrounding basins, and the location of the three principal terranes; the Talbot, Connaughton and Tabletop terranes. Modified after Bagas and Smithies (1998) and Smithies and Bagas (1997).

The Talbot Terrane, in the northwest of the Rudall Province (Fig. 3), comprises a northwesterly trending belt of multiply deformed and metamorphosed supracrustal rocks, intruded by voluminous granitic rocks of the 1804–1762 Ma Kalkan Supersuite (Hickman and Bagas, 1999; Kirkland et al., 2013a). All of these rock packages have been subsequently metamorphosed to amphibolite facies and deformed by northwest-trending folds and thrusts (Hickman and Bagas, 1999). The ages of metasedimentary rocks in the Talbot Terrane are not well constrained, but detrital zircon dating of two samples of a quartzite unit constrain at least part of the succession to be younger than 1794–1791 Ma (GSWA, 2016; Maidment, 2017). The Kalkan Supersuite intrudes the metasedimentary rocks of the Talbot Terrane as sheet-like bodies, and dominantly consists of granitic gneiss comprised of K-feldspar, quartz, plagioclase and biotite, commonly with K-feldspar augen, although more even-grained varieties are also present. Kalkan Supersuite rocks are characterized by high-K, low Sr/Y, metaluminous calc-alkaline to alkali-calcic geochemical affinities (Budd et al., 2002). Pods of serpentinized pyroxenite and dunite of unknown age are present within both the granites and the metasedimentary host rocks.

The Talbot Terrane also contains possible evidence of minor Mesoproterozoic magmatism in the region, with a biotite monzogranite yielding a U–Pb zircon date of 1453 ± 10 Ma (GSWA, 2016). Bagas (2004) interpreted this rock as evidence for a Mesoproterozoic magmatic event post-dating amphibolite-grade metamorphism. However, there is some uncertainty about the provenance of this sample, that is, whether it is *in situ*, or a transported boulder hosted by tillite of the Permian Paterson Formation (Maidment, 2017).

The Connaughton Terrane comprises metavolcanic and metasedimentary rocks which reached a metamorphic peak of upper amphibolite to granulite facies during the Parnngurr Orogeny (Anderson, 2015; Smithies and Bagas, 1997). The boundary between the Connaughton and Talbot terranes is taken to be a folded southeasterly dipping shear zone that thrusts the Connaughton Terrane over the Talbot Terrane (Bagas and Smithies, 1998). The Connaughton Terrane is distinguished from the Talbot Terrane by a higher proportion of amphibolite and mafic granulite, which are interlayered with metasedimentary rocks (Bagas and Smithies, 1998). A sample of quartzite from the terrane yields a maximum depositional age of ca. 2284 Ma, and it is possible that these rocks represent an older supracrustal succession than that exposed in the Talbot Terrane (Maidment, 2017). Like the Talbot Terrane, the Connaughton Terrane is intruded by granitic rocks of the Kalkan Supersuite, which crop out as deformed and metamorphosed gneisses. There is also evidence of minor Mesoproterozoic magmatism in the Connaughton Terrane, with a 1291 ± 10 Ma age reported for a pegmatite dyke (GSWA, 2016). A quartz–muscovite–garnet–biotite gneiss that yielded age components of 1873–1764, 1672, and 1222 Ma has been interpreted to have a ca. 1222 Ma magmatic age (GSWA, 2016), but it is also possible that these age components reflect a Paleoproterozoic granitic precursor that experienced tectonothermal events at ca. 1672 and 1222 Ma (Maidment, 2017).

The Tabletop Terrane comprises the poorly exposed eastern part of the Rudall Province. It is separated from the Connaughton Terrane by the northwesterly trending Camel–Tabletop Fault Zone (Fig. 3). Small outcrops of quartzite in the Tabletop Terrane may represent the oldest known rocks in the region, with one sample yielding a maximum depositional age of ca. 2833 Ma (Maidment, 2017).

Exposures in the Tabletop Terrane include generally weakly deformed felsic igneous rocks of the 1589–1549 Ma Krackatinny Supersuite, and actinolite–hornblende amphibolite of unknown age (Budd et al., 2002; Maidment, 2017; Smithies and Bagas, 1998). The Krackatinny Supersuite consists of fine- to medium-grained biotite–hornblende tonalites, monzogranites and leucogranites, with calcic, calc-alkaline and alkali-calcic I-type compositions (Maidment, 2017; Smithies and Bagas, 1998). Younger felsic rocks intruding the Tabletop

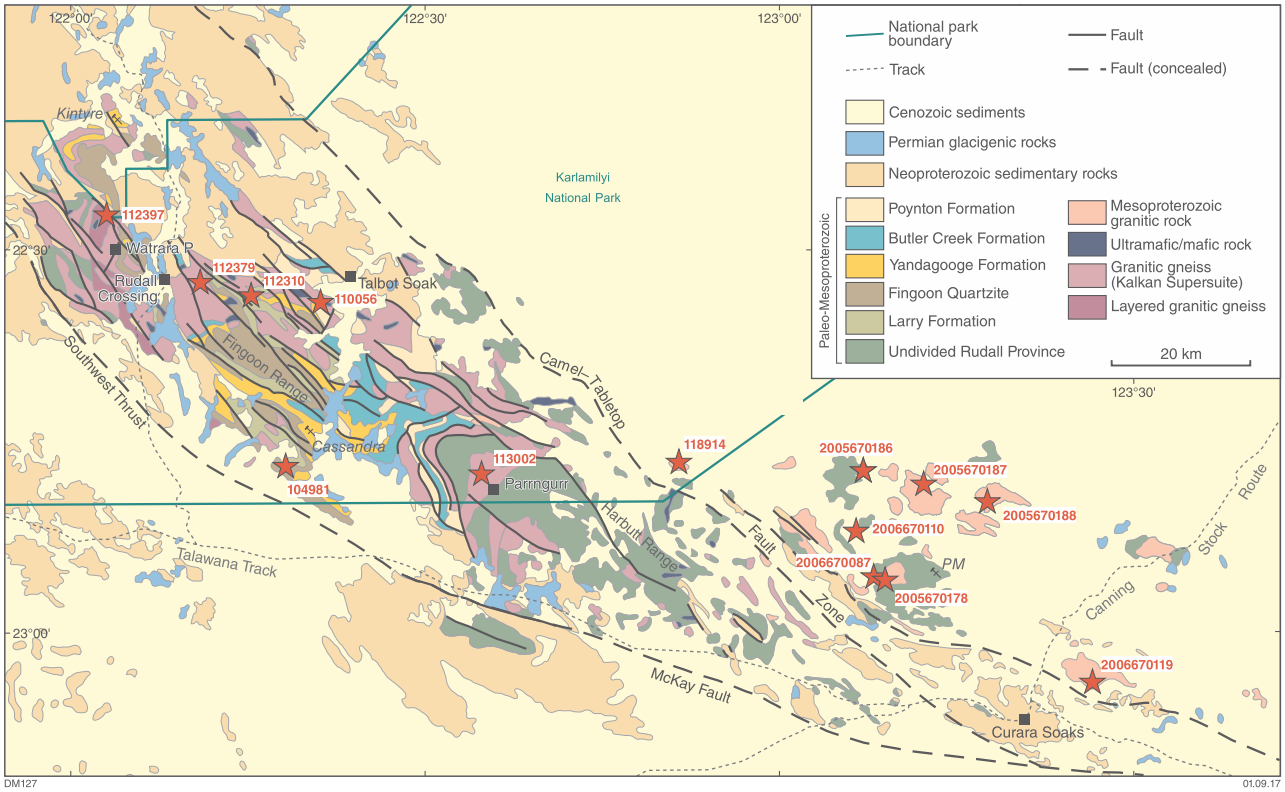

Fig. 4. Generalised outcrop geology of the Rudall province, modified from the Geoscience Australia 1:1,000,000 national surface geological map. Also indicated are the localities of the samples discussed in the text.

Terrane have been dated at 1476 ± 10 Ma (Thevissen, 1991), 1310 ± 5 Ma (GSWA, 2016), 1296 ± 4 Ma (Maidment, 2017), and 1286 ± 6 Ma (Bagas, 2004). The younger (1310–1296 Ma) felsic intrusions are dominated by leucogranite, and have been termed the Camel Suite (Maidment, 2017).

While the Talbot and Connaughton terranes share a common evolution, at least since they were intruded by the 1804–1762 Ma plutons of the Kalkan Supersuite, the poorly exposed Tabletop Terrane appears to differ to some degree, possibly reflecting spatial variations in tectonism or differential movement during Neoproterozoic deformation. No 1590–1550 Ma magmatism has yet been identified in the Talbot and Connaughton terranes, and no 1800–1760 Ma granitic rocks have yet been identified in the Tabletop Terrane, though there is limited evidence of metamorphism at ca. 1790 Ma, suggesting that the Yapungku Orogeny might have affected all three terranes (Maidment, 2017). Many outcropping igneous rocks in the Tabletop Terrane are of significantly lower metamorphic grade than those in the Talbot and Connaughton terranes (upper greenschist to lower amphibolite facies), though it is not clear to what degree the exposed rocks are representative of the terrane, since higher grade rocks do crop out at a few locations. In addition, evidence of high-grade metamorphism in the Talbot and Connaughton terranes at ca. 1688–1665 Ma and 1377–1275 Ma (Anderson, 2015; Maidment, 2017) has not yet been identified in the relatively limited dating of rocks from the Tabletop Terrane. The available evidence thus suggests that the Camel–Tabletop Fault Zone, which separates the Tabletop Terrane from the Connaughton/Talbot terranes, is a significant structure (Bagas and Lubieniecki, 2001).

Despite some differences between terranes across the Camel–Tabletop Fault Zone, the Tabletop Terrane does not appear to represent an exotic terrane, on the basis of its affinities with the western Rudall Province and the broader West Australian Craton. Detrital zircon age components from a quartzite in the Tabletop Terrane show a strong correlation with potential magmatic sources in the Pilbara Craton (Maidment, 2017), and Hf isotopic compositions of zircons from all three terranes are consistent with those obtained from other parts of the West Australian Craton (Kirkland et al., 2013b).

2.2. Duke prospect

The Duke zinc prospect (also known as Dromedary or Muttabarty) is located ~140 km north-northwest of the outcropping Rudall Province (Fig. 2). The prospect is hosted by calcareous and siliciclastic sedimentary rocks of the Neoproterozoic Yeneena Basin, which have been intruded by gabbro sills up to 380 m thick (Nifty, 2008). Portions of these sills are significantly more leucocratic and appear to represent fractionated components. The gabbro contains zones of disseminated pyrrhotite and is spatially associated with skarn-like Zn mineralization in its host rocks. It has previously been suggested that this mineralization could be related to the gabbro (Huston et al., 2010; Maidment et al., 2008), but the presence of mineralized zones within the gabbro in places suggests that this mineralizing event might instead post-date gabbro emplacement.

The nature of the basement to the Yeneena Basin in this area is uncertain as the area is entirely covered by younger sedimentary rocks. The prospect is located near the eastern margin of a domain of generally low magnetization and elevated gravity response that is bound to the east by a major fault interpreted to be an extension of the Camel–Tabletop Fault Zone. The geophysical character of the domain hosting the Duke prospect is distinct from that of the Pilbara Craton to the west, suggesting that the Yeneena Basin in this area is underlain by the Rudall Province. It is unclear whether this zone is a correlative of any of the outcropping terranes of the Province, but its position to the west of the Camel–Tabletop Fault Zone might indicate it is underlain by Talbot–Connaughton Zone correlatives.

Table 1
Summary of samples and isotope data by terrane. Quoted U–Pb magmatic ages are from the appropriate GSWA reports. εHf are simple arithmetic means of the individual analyses, while $\delta^{18}O$ is the weighted average. This is an aggregate of data from both this study[1], and from Kirkland et al. (2013b)[2] and GSWA (2016)[3]. Ages from GSWA (2016).

Suite/Supersuite	GSWA Sample No [GA Sample ID]	Lithology	Lat	Long	Age (Ma)	εHf	εNd	$\delta^{18}O$
Connaughton Terrane								
Kalkan Supersuite	113002	Granodiorite gneiss	−22.80147	122.57583	1768	−4.9[2]	−1.3	7.1[1]
Kalkan Supersuite	113035	Orthogneiss	−22.89508	122.61305	1777	−1.8[2]	−1.5	
Tabletop Terrane								
Camel Suite	118914	Foliated granite	−22.78452	122.85445	1310	−8.4[2]	−5.6	5.7[1]
Krackatinny Supersuite	GA2005670186	Monzogranite	−22.78972	123.11483	1577	−3.5[3]	−5.4	5.7[3]
Krackatinny Supersuite	GA2005670188	Monzogranite	−22.82188	123.30627	1554	−4.3[3]	−6.4	5.3[3]
Krackatinny Supersuite	GA2005670187	Quartzofeldspathic schist	−22.80259	123.20131	1549	−2.5[3]	−4.0	5.3[3]
Krackatinny Supersuite	GA2005670178	Leucogranite	−22.92867	123.14826	1589	−0.1[3]		5.7[3]
Krackatinny Supersuite	GA2006670110	Felsic veinlets in amphibolite	−22.86697	123.10577	1571	−10.9[3]		5.4[3]
Talbot Terrane								
Mesoproterozoic granite	112102	Seriate biotite metamonzogranite	−22.62091	122.12083	1453	4.1[2]	2.9	
Kalkan Supersuite	112101	Biotite-epidote monzogranite gneiss	−22.61702	122.29166	1793	−5.2[2]	−7.2	
Kalkan Supersuite	104980	Monzogranite gneiss	−22.73233	122.30067	1800	−7.9[2]	−9.2	
Kalkan Supersuite	112341	Biotite-muscovite granodiorite gneiss	−22.55919	122.17411	1773	−7.0[2]	−6.4	
Kalkan Supersuite	111843	Biotite-muscovite monzogranite gneiss	−22.57140	122.31717	1789	−8.0[2]	−5.4	
Kalkan Supersuite	111854	Biotite–muscovite granodiorite gneiss	−22.59918	122.28633	1782	−6.4[2]		
Kalkan Supersuite	112310	Granodiorite gneiss	−22.56113	122.28161	1801	−2.7[2]	−4.1	6.1[1]
Kalkan Supersuite	112379	Biotite monzogranite (augen) gneiss	−22.53752	122.18105	1762	−7.8[2]		6.8[1]
Kalkan Supersuite	112397	Biotite monzogranite (augen) gneiss	−22.46946	122.06106	1783	−6.8[2]	−3.2	7.4[1]
Kalkan Supersuite	104981	Biotite-muscovite monzogranite gneiss	−22.77444	122.25917	1764	−6.0[2]	−2.4	6.6[1]
Kalkan Supersuite	110056	Biotite–hornblende granodiorite gneiss	−22.56808	122.35800	1795	−4.4[2]	−4.6	8.0[1]
Duke gabbro	GA2005677310-22	Leucocratic phase within gabbroic intrusion	−21.38607	121.60372	831	−2.5[1]		6.5[1]

3. Samples and previous U–Pb and Lu–Hf results

We report new zircon O isotope data from seven samples (all previously dated by SHRIMP zircon U–Pb geochronology; see below) from granitic suites across the three terranes (Connaughton, Tabletop and Talbot). We also report new zircon U–Pb, Lu–Hf and O isotope data from a leucocratic phase of a gabbroic intrusion at the Duke prospect (Fig. 4). The new isotope data presented here complement existing zircon Lu–Hf and U–Pb, and whole-rock Sm–Nd, isotopic datasets for the magmatic suites of the Rudall Province (Hickman and Bagas, 1999; Kirkland et al., 2013b; Maidment, 2017), and together provide a substantial isotopic dataset. Table 1 details the new samples analyzed in this study, as well as samples with existing data compiled herein, which are shown on a map in Fig. 4. Sample numbers are those assigned by the Geological Survey of Western Australia (GSWA) unless otherwise indicated; Sample IDs assigned by Geoscience Australia are prefixed 'GA'.

Zircon Hf isotope data were collected for five samples from the Talbot Terrane, all of which are assigned to the Kalkan Supersuite (Fig. 4). These samples have yielded previous zircon U–Pb geochronologic data (GSWA, 2016), and zircon Lu-Hf isotope analysis (Kirkland et al., 2013b). Some of the U–Pb dates have been recalculated by Kirkland et al. (2013b), resulting in minor changes compared with original published dates. U–Pb magmatic ages are weighted mean $^{207}Pb/^{206}Pb$ dates, and εHf values are calculated from each individual Lu–Hf analysis using the mean U–Pb magmatic age of the rock. All uncertainties are cited at 2σ throughout.

Within the Connaughton Terrane, one sample from the Kalkan Supersuite, 113002, was analyzed for zircon O isotopes. We also report new zircon O isotope data for one sample from the Tabletop Terrane; the Camel Suite, sample 118914, which has a magmatic age of 1310 ± 5 Ma. Sample GA 2005677310-22 is a leucocratic phase of a gabbro intrusion, sampled from a drillcore in the Duke prospect. Its magmatic U-Pb age has previously been cited as 831 ± 6 Ma (Maidment et al., 2008), and here we report the underlying zircon U-Pb data, as well as new Lu-Hf and O isotope data for this sample.

4. Results

4.1. Analytical techniques

The Duke Prospect sample GA 2005677310-22, was analyzed for zircon U-Pb geochronology by Geoscience Australia using SHRIMP-IIB, within the John de Laeter Centre for Mass Spectrometry at Curtin University. Zircons for which Lu–Hf isotope data are available were analyzed using a NewWave/Merchantek LUV 213 laser ablation microprobe, attached to a Nu Plasma multi-collector inductively coupled plasma mass spectrometer (LA-MC-ICP-MS) at Macquarie University. All but one of these Lu–Hf datasets were presented by Kirkland et al. (2013b); the exception is Duke Prospect sample GA 2005677310-22, for which new data are reported below.

Zircon oxygen isotope ratios, $^{18}O/^{16}O$ and $^{16}OH/^{16}O$, were determined using the large geometry Cameca 1280 multi-collector ion microprobe facility at the Centre for Microscopy, Characterization and Analysis (CMCA) at the University of Western Australia. All oxygen isotope data are reported relative to Vienna Standard Mean Ocean Water (V-SMOW). Full details of the analytical methods are supplied in the Methods section, and U-Pb, O and Lu-Hf isotope results are detailed in Tables 2–4 respectively.

4.2. Zircon U-Pb geochronology of the Duke gabbro

The Duke gabbro yielded euhedral, colourless zircon crystals. The grains are up to 200 μm long, equant to moderately elongate in shape. The crystals display either broad concentric growth zoning or uniform cathodoluminescence emission. This sample was analyzed over two sessions, both on 23 January 2006. Analyses 2.1–15.1 (spot numbers 1–14) were obtained during the first session, together with 15 analyses of the TEMORA2 standard, which indicated an external spot-to-spot (reproducibility) uncertainty of 1.19% (1σ) and a $^{238}U/^{206}Pb^*$ calibration uncertainty of 0.35% (1σ). Analyses 16.1 to 29.1 (spot numbers 15–28) were obtained during the second session, together with 13 analyses of the TEMORA2 standard, which indicated an external spot-to-spot (reproducibility) uncertainty of 0.71% (1σ) and a $^{238}U/^{206}Pb^*$ calibration uncertainty of 0.26% (1σ). Calibration uncertainties are

Table 2
Ion microprobe U-Pb analytical results for zircons from sample GA 2005677310-22 (Duke gabbro). All errors are at the 1σ level. f204% is the percentage of common ^{206}Pb, estimated from the measured ^{204}Pb. Spot no. refers to the sequential order of analysis. Grain.spot is the individual grain and analysis identification. Age calculations use the routines of Ludwig (2004) and follow the decay constant recommendations of Steiger and Jager (1977). Group ID refers to the following interpretations; I = magmatic; P = Pb loss. Disc (%) is the age discordance as defined = 100 × (1 − [(^{238}U/^{206}Pb date)/(^{207}Pb/^{206}Pb date)]).

Group ID	Spot no	Grain spot.	^{238}U (ppm)	^{232}Th (ppm)	^{232}Th/^{238}U	f204 (%)	^{238}U/^{206}Pb	± 1σ	^{207}Pb/^{206}Pb	± 1σ	^{238}U/^{206}Pb*	± 1σ	^{207}Pb*/^{206}Pb*	± 1σ	^{238}U/^{206}Pb*date (Ma)	± 1σ	^{207}Pb*/^{206}Pb*date (Ma)	± 1σ	Disc. (%)
I	1	W2.1	1455	2146	1.52	0.019	7.319	0.088	0.06665	0.00018	7.320	0.092	0.06649	0.00019	825	10	822	6	−0.4
I	2	W3.1	1202	1780	1.53	0.003	7.351	0.089	0.06667	0.00020	7.351	0.093	0.06665	0.00020	822	10	827	6	0.6
I	3	W4.1	921	1241	1.39	0.038	7.398	0.090	0.06728	0.00022	7.401	0.094	0.06697	0.00024	817	10	837	7	2.4
I	4	W5.1	1385	2182	1.63	0.017	7.326	0.088	0.06673	0.00017	7.327	0.092	0.06659	0.00018	825	10	825	6	0.0
I	5	W6.1	1371	2162	1.63	0.013	7.368	0.089	0.06723	0.00018	7.369	0.093	0.06712	0.00019	820	10	842	6	2.5
I	6	W7.1	1135	1567	1.43	0.013	7.387	0.089	0.06699	0.00020	7.388	0.093	0.06688	0.00020	818	10	834	6	1.9
I	7	W8.1	1255	1895	1.56	−0.009	7.408	0.092	0.06694	0.00019	7.407	0.096	0.06701	0.00019	816	10	838	6	2.6
I	8	W9.1	1027	1444	1.45	0.063	7.418	0.090	0.06709	0.00021	7.423	0.094	0.06657	0.00023	815	10	824	7	1.2
I	9	W10.1	1726	2857	1.71	0.018	7.336	0.088	0.06671	0.00018	7.338	0.092	0.06656	0.00018	824	10	824	6	0.1
I	10	W11.1	2091	3933	1.94	0.012	7.324	0.088	0.06673	0.00018	7.325	0.092	0.06663	0.00018	825	10	826	6	0.2
I	11	W12.1	1396	2235	1.65	0.065	7.463	0.090	0.06724	0.00018	7.468	0.094	0.06670	0.00021	810	9	828	6	2.2
I	12	W13.1	1174	1726	1.52	0.001	7.548	0.091	0.06701	0.00024	7.548	0.095	0.06700	0.00024	802	9	838	8	4.3
P	13	W14.1	389	327	0.87	0.031	7.513	0.093	0.06675	0.00034	7.515	0.097	0.06649	0.00035	805	10	822	11	2.0
I	14	W15.1	1245	1733	1.44	0.017	7.462	0.091	0.06690	0.00019	7.463	0.095	0.06676	0.00020	811	10	830	6	2.4
I	15	W16.1	1205	1585	1.36	0.026	7.171	0.057	0.06691	0.00019	7.172	0.059	0.06670	0.00020	841	6	828	6	−1.6
I	16	W17.1	1644	2599	1.63	0.012	7.176	0.056	0.06678	0.00014	7.177	0.059	0.06667	0.00015	841	6	828	5	−1.6
I	17	W18.1	2127	4079	1.98	0.005	7.217	0.055	0.06665	0.00019	7.217	0.058	0.06661	0.00019	837	6	826	6	−1.3
I	18	W19.1	1093	1590	1.50	0.016	7.270	0.058	0.06724	0.00018	7.271	0.061	0.06710	0.00019	831	6	841	6	1.2
I	19	W20.1	957	1272	1.37	0.021	7.235	0.054	0.06695	0.00026	7.236	0.057	0.06677	0.00027	834	6	831	9	−0.5
I	20	W21.1	1212	1793	1.53	0.025	7.288	0.054	0.06706	0.00017	7.290	0.057	0.06686	0.00018	829	6	833	6	0.6
I	21	W22.1	1037	1450	1.44	0.011	7.313	0.055	0.06704	0.00020	7.314	0.058	0.06695	0.00021	826	6	836	6	1.2
I	22	W23.1	2232	3196	1.48	0.015	7.190	0.053	0.06697	0.00012	7.191	0.056	0.06685	0.00013	839	6	833	4	−0.8
I	23	W24.1	1282	1608	1.30	0.003	7.204	0.057	0.06669	0.00016	7.205	0.060	0.06666	0.00016	838	6	827	5	−1.3
I	24	W25.1	2384	4757	2.06	0.006	7.094	0.057	0.06674	0.00012	7.094	0.060	0.06668	0.00013	850	7	828	4	−2.7
I	25	W26.1	2078	4049	2.01	0.012	7.242	0.056	0.06679	0.00013	7.243	0.059	0.06669	0.00013	834	6	828	4	−0.7
I	26	W27.1	1369	1936	1.46	0.001	7.244	0.057	0.06704	0.00016	7.244	0.060	0.06703	0.00016	834	6	839	5	0.6
I	27	W28.1	806	927	1.19	0.016	7.310	0.060	0.06717	0.00021	7.311	0.063	0.06704	0.00022	826	7	839	7	1.5
I	28	W29.1	3338	8348	2.58	0.006	7.067	0.053	0.06668	0.00010	7.067	0.056	0.06663	0.00011	853	6	826	3	−3.2

Table 3
Zircon Lu–Hf isotope data for samples from the Rudall Province.

Analysis No	$^{176}Hf/^{177}Hf$	1SE	$^{176}Lu/^{177}Hf$	$^{176}Yb/^{177}Hf$	$^{176}Hf/^{177}Hf_i$	εHf	1SE	T_{DM} (Ga)	T_{DM}^2 (Ga)
DUKE-02.1	0.282247	0.000007	0.003636	0.16090	0.282191	-2.54	0.24	1.53	1.88
DUKE-03.1	0.282252	0.000020	0.003981	0.19349	0.282191	-2.63	0.70	1.53	1.89
DUKE-04.1	0.282228	0.000009	0.004153	0.19939	0.282165	-3.67	0.33	1.58	1.95
DUKE-05.1	0.282249	0.000014	0.004676	0.22394	0.282177	-3.05	0.49	1.57	1.92
DUKE-06.1	0.282177	0.000019	0.005771	0.23755	0.282089	-6.29	0.67	1.73	2.12
DUKE-07.1	0.282261	0.000008	0.004047	0.17669	0.282199	-2.40	0.29	1.52	1.87
DUKE-08.1	0.282249	0.000012	0.004141	0.19339	0.282186	-2.94	0.42	1.54	1.90
DUKE-10.1	0.282248	0.000013	0.005634	0.26065	0.282162	-3.63	0.46	1.62	1.95
DUKE-11.1	0.282216	0.000010	0.006853	0.32543	0.282111	-5.40	0.35	1.73	2.06
DUKE-12.1	0.282268	0.000011	0.003828	0.18463	0.282210	-2.21	0.39	1.50	1.85
DUKE-13.1	0.282209	0.000014	0.004935	0.23278	0.282136	-5.04	0.49	1.64	2.02
DUKE-15.1	0.282265	0.000010	0.003877	0.17500	0.282207	-2.33	0.35	1.51	1.86
DUKE-16.1	0.282269	0.000009	0.002378	0.10291	0.282231	-0.56	0.32	1.44	1.78
DUKE-24.1	0.282268	0.000007	0.002106	0.09518	0.282235	-0.50	0.23	1.43	1.77
DUKE-26.1	0.282279	0.000017	0.002014	0.09532	0.282247	-0.15	0.60	1.41	1.75
DUKE-27.1	0.282289	0.000015	0.003020	0.12229	0.282242	-0.37	0.52	1.44	1.76
DUKE-28.1	0.282262	0.000007	0.003556	0.15313	0.282207	-1.76	0.24	1.50	1.84
DUKE-29.1	0.282286	0.000009	0.002750	0.12646	0.282242	0.08	0.33	1.43	1.75

included in the errors of $^{238}U/^{206}Pb^*$ ratios and dates listed in Table 1. Common-Pb corrections were applied to all analyses using contemporaneous isotopic compositions determined according to the model of Stacey and Kramers (1975).

Twenty-eight analyses were obtained from 28 zircons. Results are listed in Table 2 and shown in a concordia diagram (Fig. 5). The analyses cluster around Concordia, and range from −3 to +4% discordant (Fig. 5). The 28 analyses can be divided into two groups, based on their $^{207}Pb^*/^{206}Pb^*$ and $^{238}U/^{206}Pb^*$ ratios. Group I comprises 27 analyses (Table 2) with very high to extreme U (806–3338 ppm, median 1282 ppm), Th (927–8348 ppm, median 1835 ppm) and Th/U (1.19–2.58, median 1.52), which yielded a Concordia age of 831 ± 2.2 Ma (2σ; MSWD = 1.6). Group P comprises a single analysis (Table 2) with markedly lower U (389 ppm), Th (327 ppm) and Th/U (0.87), which yielded a marginally younger age ($^{238}U/^{206}Pb^*$ = 805 ± 19 Ma (2σ) and $^{207}Pb^*/^{206}Pb^*$ = 822 ± 22 Ma (2σ)). The date of 831 ± 4 Ma for 27 analyses in Group I is interpreted as the age of magmatic crystallization of this leucocratic phase. The single analysis in Group P is interpreted to have been affected by a post-magmatic recrystallization event, resulting in partial expulsion of U and Th from the crystal lattice, and it is likely that at least some radiogenic Pb was lost at this time.

4.3. Lu–Hf isotopes

Eighteen Hf isotope analyses from the Duke leucocratic gabbro yielded a minimum εHf of −6.3, and a maximum of 0.0, with a mean εHf of 2.5 ± 3.6 (2σ). Using a $^{176}Lu/^{177}Hf$ ratio of 0.015 for average continental crust, these resolve to two-stage Hf model ages (T_{DM}^2) of between 1.75 and 2.12 Ga, with an average of 1.88 Ga (Fig. 7).

4.4. O isotopes

4.4.1. O–OH data

Water in zircon ($^{16}O^1H/^{16}O$) was measured simultaneously with O isotopes ($^{18}O/^{16}O$) as a means to assess whether the oxygen signature was a primary magmatic feature of the zircon crystal, or has been affected by secondary alteration. Aines and Rossman (1986) established a relationship between zircon radiation damage and trace amounts of water. $^{16}O^1H/^{16}O$ content is typically high in a metamict crystal, since water is able to enter into the crystal lattice to balance charge defects (Van Kranendonk et al., 2015). In contrast, water content approaches zero in pristine zircon crystals. Thus, $^{16}O^1H/^{16}O$ observed in zircon compared to that in the standard can be regarded as a measure of crystal damage, and therefore an indicator of suspect O data. In the Rudall oxygen isotope dataset, we observe a correlation between a subset of heavy $\delta^{18}O$ analysis and elevated water content (Fig. 6). We therefore apply a cutoff value of $^{16}O^1H/^{16}O \approx 0.006$ determined on the basis of excluding those $\delta^{18}O$ analyses (n = 6) plotting at high $^{16}O^1H/^{16}O$ values which we interpret as reflecting secondary values. Across the total dataset of 181 individual O analyses presented herein, this cutoff affects two analysis of the Camel Suite (sample 118914), one analysis of Kalkan Supersuite sample 104981, and three on sample 110056, also of the Kalkan Supersuite.

Interestingly, elevated $^{16}O^1H/^{16}O$ values are consistently correlated with anomalously heavy $\delta^{18}O$. Pidgeon et al. (2013) also noted a relationship between elevated $^{16}O^1H/^{16}O$ and secondary $\delta^{18}O$ signatures, but found no consistent correlation between $\delta^{18}O$ deviations to heavier isotopic values, and suggested that these trends could reflect variations in the hydration or hydrolysis processes taking place due to inhomogeneity in the metamict zircon.

4.4.2. O isotope results

Oxygen isotope analysis was performed on zircon grains from five samples of the Kalkan Supersuite, Talbot Terrane (sample nos. 112310, 121379, 112397, 104981, 110056). Twenty analyses of sample 112310 revealed a range in $\delta^{18}O$ from 5.2 to 7.1‰. A weighted mean for 112310 with no exclusions gave a $\delta^{18}O$ of 6.2 ± 0.5‰ (2σ; MSWD 3.3). Twenty analyses of sample 112379 ranged in $\delta^{18}O$ from 6.5 to 7.6‰. A weighted mean for 112379 with no exclusions gave a $\delta^{18}O$ of 6.8 ± 0.2‰ (2σ; MSWD 1.1). Sixteen analyses of sample 112397 gave a minimum $\delta^{18}O$ of 6.3‰ and a maximum of 7.9‰. A weighted mean for 112397 with no exclusions gave a $\delta^{18}O$ of 7.4 ± 0.4‰ (2σ; MSWD 2.1). Nineteen analyses of sample 104981 gave a range in $\delta^{18}O$ from 5.6 to 8.0‰. A weighted mean for 104981 excluding one analysis with an anomalously high OH/O value gave a $\delta^{18}O$ of 6.4 ± 0.5‰ (2σ; MSWD 4.0). Seventeen analyses of sample 110056 had a range in $\delta^{18}O$ from 3.8 to 9.4‰. A weighted mean for 110056 excluding three analyses with anomalously high OH/O values gave a $\delta^{18}O$ of 7.3 ± 1.6‰ (2σ; MSWD 38). This last sample showed the widest range in $\delta^{18}O$ of all samples analyzed. Taken together, the oxygen isotope data from the Kalkan Supersuite in the Talbot terrane ranges in $\delta^{18}O$ from 3.8‰ to 12.6‰, with a mean of 6.95 ± 2.4‰ (2σ).

Oxygen isotope analysis was also performed on zircon separates from one sample of the Kalkan Supersuite from the Connaughton Terrane (sample 113002). Sixteen analyses gave a range in $\delta^{18}O$ from 6.62 to 9.30‰. A weighted mean for 113002 gave a $\delta^{18}O$ of 7.2 ± 0.7‰ (2σ; MSWD 1.3).

Oxygen isotope analysis was performed on zircon grains from a single sample of the Camel Suite (sample 118914), of the Tabletop

Table 4
Zircon oxygen isotope data for samples from the Rudall Province. 'ex' refers to analyses excluded on the basis of OH/O ratio.

Analysis name	SIMS corrected ratios		Delta values			
	$^{18}O/^{16}O$	2σ abs	$\delta^{18}O$	2σ abs	$^{16}O^{1}H/^{16}O$	2σ abs
Kalkan Supersuite						
SAMPLE 110056						
110056@01	0.0020154	0.0000010	5.10	0.48	0.0007186	0.0000010
110056@06	0.0020128	0.0000010	3.81	0.50	0.0016399	0.0000023
110056@10	0.0020185	0.0000010	6.64	0.51	0.0006641	0.0000004
110056@11	0.0020231	0.0000010	8.92	0.52	0.0042456	0.0000400
110056@12	0.0020215	0.0000010	8.14	0.53	0.0007681	0.0000013
110056@13	0.0020204	0.0000010	7.56	0.51	0.0012025	0.0000012
110056@14	0.0020180	0.0000010	6.41	0.53	0.0006048	0.0000004
110056@15	0.0020197	0.0000010	7.24	0.51	0.0021632	0.0000102
110056@16 (ex)	0.0020305	0.0000010	12.61	0.48	0.0106180	0.0000059
110056@17	0.0020198	0.0000010	7.29	0.55	0.0011753	0.0000024
110056@18	0.0020240	0.0000010	9.35	0.51	0.0038743	0.0000025
110056@19 (ex)	0.0020290	0.0000010	11.87	0.50	0.0150490	0.0000064
110056@2 (ex)	0.0020251	0.0000010	9.94	0.53	0.0072213	0.0000086
110056@20	0.0020227	0.0000010	8.75	0.52	0.0060411	0.0000115
110056@3	0.0020188	0.0000010	6.78	0.53	0.0011331	0.0000014
110056@4	0.0020241	0.0000012	9.44	0.62	0.0010476	0.0000016
110056@5	0.0020238	0.0000012	9.29	0.56	0.0008619	0.0000003
110056@7	0.0020201	0.0000010	7.44	0.52	0.0009694	0.0000021
110056@8	0.0020207	0.0000010	7.71	0.52	0.0005965	0.0000004
110056@9	0.0020159	0.0000010	5.31	0.48	0.0004855	0.0000003
SAMPLE 104981						
104981@01	0.0020187	0.0000010	6.72	0.52	0.0005668	0.0000003
104981@06	0.0020183	0.0000010	6.53	0.52	0.0012273	0.0000037
104981@10	0.0020180	0.0000010	6.39	0.54	0.0006129	0.0000007
104981@11	0.0020181	0.0000012	6.42	0.56	0.0008968	0.0000023
104981@12	0.0020187	0.0000010	6.73	0.49	0.0005982	0.0000008
104981@13	0.0020179	0.0000012	6.31	0.56	0.0006474	0.0000007
104981@14	0.0020164	0.0000010	5.57	0.54	0.0007693	0.0000141
104981@15	0.0020172	0.0000012	5.99	0.57	0.0008500	0.0000021
104981@16 (ex)	0.0020252	0.0000010	9.98	0.50	0.0108870	0.0000237
104981@17	0.0020174	0.0000010	6.10	0.49	0.0008998	0.0000051
104981@18	0.0020179	0.0000010	6.33	0.52	0.0008040	0.0000007
104981@19	0.0020169	0.0000010	5.85	0.50	0.0008095	0.0000029
104981@2	0.0020213	0.0000010	8.03	0.50	0.0053563	0.0000270
104981@20	0.0020183	0.0000010	6.55	0.54	0.0010939	0.0000012
104981@3	0.0020176	0.0000010	6.20	0.49	0.0007831	0.0000008
104981@4	0.0020174	0.0000010	6.10	0.50	0.0005845	0.0000006
104981@5	0.0020192	0.0000010	6.99	0.53	0.0025482	0.0000089
104981@7	0.0020181	0.0000010	6.43	0.49	0.0008427	0.0000698
104981@8	0.0020182	0.0000010	6.47	0.49	0.0007785	0.0000063
104981@9	0.0020181	0.0000010	6.43	0.53	0.0009295	0.0000026
SAMPLE 112310						
112310@01	0.0020162	0.0000010	5.49	0.48	0.0013313	0.0000022
112310@06	0.0020195	0.0000009	7.12	0.46	0.0025634	0.0000013
112310@10	0.0020172	0.0000009	5.99	0.46	0.0011499	0.0000016
112310@11	0.0020175	0.0000010	6.14	0.48	0.0008136	0.0000015
112310@12	0.0020179	0.0000010	6.35	0.48	0.0004278	0.0000004
112310@13	0.0020185	0.0000009	6.63	0.46	0.0005318	0.0000004
112310@14	0.0020175	0.0000009	6.13	0.46	0.0008651	0.0000018
112310@15	0.0020193	0.0000009	7.05	0.44	0.0048183	0.0000066
112310@16	0.0020180	0.0000010	6.38	0.49	0.0010945	0.0000039
112310@17	0.0020185	0.0000009	6.62	0.46	0.0003871	0.0000003
112310@18	0.0020168	0.0000010	5.79	0.48	0.0009806	0.0000016
112310@19	0.0020183	0.0000009	6.55	0.47	0.0023546	0.0000020
112310@2	0.0020156	0.0000009	5.18	0.46	0.0015470	0.0000038
112310@20	0.0020168	0.0000010	5.76	0.49	0.0008777	0.0000006
112310@3	0.0020158	0.0000009	5.27	0.46	0.0006183	0.0000018
112310@4	0.0020176	0.0000009	6.20	0.46	0.0006675	0.0000006
112310@5	0.0020190	0.0000009	6.88	0.45	0.0021893	0.0000029
112310@7	0.0020167	0.0000010	5.73	0.48	0.0006622	0.0000020
112310@8	0.0020171	0.0000010	5.95	0.48	0.0025213	0.0000032
112310@9	0.0020164	0.0000009	5.57	0.47	0.0017645	0.0000014
SAMPLE 113002						
113002@01	0.0020187	0.0000009	6.71	0.46	0.0004626	0.0000027
113002@06	0.0020200	0.0000009	7.39	0.47	0.0003564	0.0000004
113002@10	0.0020186	0.0000009	6.68	0.45	0.0004254	0.0000004
113002@11	0.0020201	0.0000009	7.43	0.47	0.0003542	0.0000003
113002@12	0.0020192	0.0000009	6.99	0.47	0.0004708	0.0000005
113002@13	0.0020189	0.0000010	6.82	0.47	0.0004869	0.0000032

(*continued on next page*)

Table 4 (*continued*)

Analysis name	SIMS corrected ratios		Delta values			
	$^{18}O/^{16}O$	2σ abs	$\delta^{18}O$	2σ abs	$^{16}O^{1}H/^{16}O$	2σ abs
113002@14	0.0020193	0.0000009	7.03	0.47	0.0005000	0.0000006
113002@15	0.0020185	0.0000009	6.62	0.46	0.0004511	0.0000011
113002@16	0.0020191	0.0000010	6.94	0.51	0.0004192	0.0000023
113002@2	0.0020198	0.0000009	7.29	0.47	0.0004326	0.0000004
113002@3	0.0020187	0.0000009	6.71	0.46	0.0006286	0.0000010
113002@4	0.0020238	0.0000010	9.30	0.49	0.0004892	0.0000003
113002@5	0.0020222	0.0000009	8.47	0.46	0.0005022	0.0000003
113002@7	0.0020196	0.0000010	7.20	0.50	0.0010813	0.0000053
113002@8	0.0020193	0.0000009	7.03	0.47	0.0004367	0.0000003
113002@9	0.0020193	0.0000010	7.05	0.51	0.0004581	0.0000002
SAMPLE 112379						
112379@06	0.0020183	0.0000010	6.54	0.51	0.0009388	0.0000032
112379@07	0.0020194	0.0000010	7.08	0.47	0.0013056	0.0000018
112379@08	0.0020190	0.0000010	6.88	0.49	0.0010281	0.0000036
112379@09	0.0020187	0.0000010	6.74	0.49	0.0009589	0.0000035
112379@1	0.0020185	0.0000010	6.65	0.48	0.0012983	0.0000044
112379@10	0.0020183	0.0000010	6.55	0.49	0.0008475	0.0000019
112379@11	0.0020191	0.0000010	6.94	0.48	0.0012036	0.0000031
112379@12	0.0020186	0.0000010	6.66	0.49	0.0008917	0.0000019
112379@13	0.0020186	0.0000010	6.66	0.52	0.0012103	0.0000030
112379@14	0.0020191	0.0000010	6.93	0.48	0.0009314	0.0000025
112379@15	0.0020187	0.0000010	6.75	0.49	0.0009321	0.0000024
112379@16	0.0020183	0.0000010	6.53	0.53	0.0010016	0.0000027
112379@17	0.0020182	0.0000012	6.47	0.60	0.0011599	0.0000026
112379@18	0.0020190	0.0000010	6.90	0.49	0.0024156	0.0000057
112379@19	0.0020191	0.0000010	6.93	0.49	0.0008305	0.0000017
112379@2	0.0020183	0.0000010	6.55	0.50	0.0008866	0.0000026
112379@20	0.0020190	0.0000010	6.90	0.50	0.0008183	0.0000018
112379@3	0.0020182	0.0000010	6.48	0.50	0.0011940	0.0000028
112379@4	0.0020185	0.0000010	6.63	0.49	0.0009385	0.0000019
112379@5	0.0020203	0.0000010	7.55	0.49	0.0009113	0.0000022
SAMPLE 112397						
112397@01	0.0020209	0.0000010	7.85	0.52	0.0009330	0.0000011
112397@02	0.0020205	0.0000010	7.65	0.51	0.0011495	0.0000128
112397@03	0.0020208	0.0000010	7.79	0.48	0.0010267	0.0000108
112397@04	0.0020196	0.0000010	7.19	0.52	0.0008985	0.0000015
112397@05	0.0020209	0.0000012	7.82	0.61	0.0009001	0.0000019
112397@06	0.0020199	0.0000010	7.33	0.48	0.0009355	0.0000018
112397@07	0.0020198	0.0000010	7.29	0.49	0.0010541	0.0000005
112397@08	0.0020197	0.0000010	7.21	0.50	0.0008469	0.0000017
112397@09	0.0020203	0.0000010	7.55	0.50	0.0008721	0.0000017
112397@10	0.0020207	0.0000010	7.72	0.49	0.0010557	0.0000003
112397@11	0.0020200	0.0000010	7.36	0.52	0.0008635	0.0000008
112397@12	0.0020199	0.0000010	7.32	0.48	0.0010438	0.0000011
112397@13	0.0020197	0.0000010	7.25	0.48	0.0008560	0.0000012
112397@14	0.0020179	0.0000010	6.34	0.55	0.0011051	0.0000089
112397@15	0.0020199	0.0000010	7.31	0.48	0.0008113	0.0000010
112397@16	0.0020209	0.0000010	7.84	0.47	0.0008198	0.0000016
Camel Suite						
SAMPLE 118914						
118914@01	0.0020213	0.0000012	8.02	0.55	0.0034637	0.0000200
118914@02	0.0020165	0.0000012	5.61	0.57	0.0029125	0.0000042
118914@03	0.0020142	0.0000012	4.51	0.56	0.0022171	0.0000404
118914@04	0.0020142	0.0000012	4.51	0.58	0.0013427	0.0000036
118914@05	0.0020151	0.0000012	4.92	0.58	0.0016178	0.0000064
118914@06	0.0020176	0.0000012	6.18	0.62	0.0054877	0.0000024
118914@07 (ex)	0.0020213	0.0000012	8.02	0.57	0.0081777	0.0000040
118914@08	0.0020159	0.0000012	5.31	0.57	0.0014833	0.0000009
118914@09	0.0020160	0.0000012	5.38	0.57	0.0052210	0.0000499
118914@10	0.0020157	0.0000012	5.23	0.59	0.0009002	0.0000007
118914@11	0.0020161	0.0000012	5.44	0.56	0.0031220	0.0000555
118914@12 (ex)	0.0020162	0.0000012	5.51	0.57	0.0075739	0.0000786
118914@13	0.0020157	0.0000012	5.25	0.56	0.0011527	0.0000045
118914@14	0.0020153	0.0000012	5.04	0.56	0.0030796	0.0000053
118914@15	0.0020185	0.0000012	6.64	0.57	0.0059591	0.0000039
118914@16	0.0020166	0.0000012	5.69	0.58	0.0027679	0.0000041
118914@17	0.0020163	0.0000012	5.52	0.55	0.0015488	0.0000019
118914@18	0.0020159	0.0000010	5.33	0.55	0.0008718	0.0000016
Duke gabbro						
SAMPLE DUKE						
DUKE@1	0.0020179	0.0000010	6.34	0.48	0.0029031	0.0000041

(*continued on next page*)

Table 4 (*continued*)

Analysis name	SIMS corrected ratios		Delta values			
	$^{18}O/^{16}O$	2σ abs	$\delta^{18}O$	2σ abs	$^{16}O^{1}H/^{16}O$	2σ abs
DUKE@10	0.0020192	0.0000009	6.96	0.47	0.0006299	0.0000007
DUKE@12	0.0020184	0.0000010	6.60	0.51	0.0006813	0.0000005
DUKE@13	0.0020185	0.0000010	6.65	0.50	0.0010254	0.0000005
DUKE@14	0.0020186	0.0000009	6.66	0.47	0.0006798	0.0000012
DUKE@16	0.0020180	0.0000012	6.38	0.62	0.0006680	0.0000004
DUKE@17	0.0020175	0.0000010	6.12	0.52	0.0007209	0.0000008
DUKE@18	0.0020173	0.0000010	6.04	0.49	0.0006884	0.0000007
DUKE@19	0.0020177	0.0000009	6.24	0.47	0.0006888	0.0000007
DUKE@2	0.0020183	0.0000011	6.55	0.53	0.0008788	0.0000005
DUKE@20	0.0020181	0.0000010	6.43	0.50	0.0005080	0.0000005
DUKE@3	0.0020188	0.0000010	6.76	0.48	0.0007696	0.0000004
DUKE@4	0.0020190	0.0000009	6.86	0.46	0.0006683	0.0000008
DUKE@6	0.0020171	0.0000010	5.94	0.49	0.0007017	0.0000005
DUKE@8	0.0020179	0.0000013	6.33	0.64	0.0006606	0.0000003
DUKE@9	0.0020182	0.0000010	6.46	0.49	0.0008011	0.0000005

Terrane. Sixteen analyses showed a range in $\delta^{18}O$ from 4.5 to 8.0‰. A weighted mean for 118914, excluding two analyses with anomalously high OH/O values, gave a $\delta^{18}O$ of 5.5 ± 1.0‰ (2σ; MSWD 3.4). Oxygen isotope analysis was also performed on zircon separates from the Duke leucocratic gabbro. Sixteen analyses have a range in $\delta^{18}O$ from 5.9 to 7.0‰. A weighted mean with no exclusions gave a $\delta^{18}O$ of 6.5 ± 0.4‰ (2σ; MSWD 1.4).

5. Discussion

For discussion, we subdivide the Rudall Province isotope dataset, comprising data reported here and those from previous studies (Kirkland et al., 2013b), on a terrane and magmatic suite basis. The Kalkan Supersuite intrudes both the Connaughton and Talbot terranes, and data from the two terranes are here treated separately for discussion. Table 1 summarizes the isotope characteristics of the samples by terrane and (super)suite.

5.1. Crustal evolution trends of the Rudall Province

A Hf evolution diagram plots magmatic age against εHf, measured within the same zircon grain, and allows the discrimination of magmatic source trends through time. Fig. 7 shows a Hf evolution plot for the Rudall Province magmatic suites, annotated by terrane, and includes analyses of both magmatic zircons and pre-1800 Ma xenocrysts. The majority of analyzed igneous rocks from the Rudall Province have evolved zircon Hf isotopic signatures (negative εHf). These samples include those from the Connaughton and Tabletop terranes, and the Kalkan Supersuite of the Talbot Terrane. These evolved Hf values imply that magmatism was largely derived from the reworking of existing, perhaps heterogeneous, crustal material, with limited input of external juvenile material. The Krackatinny Supersuite (Tabletop Terrane) presents the greatest range in εHf, spanning some 20 epsilon units from slightly juvenile to highly evolved values, within a relatively narrow time interval (~40 Ma) (Fig. 7), suggesting that its magmatism was

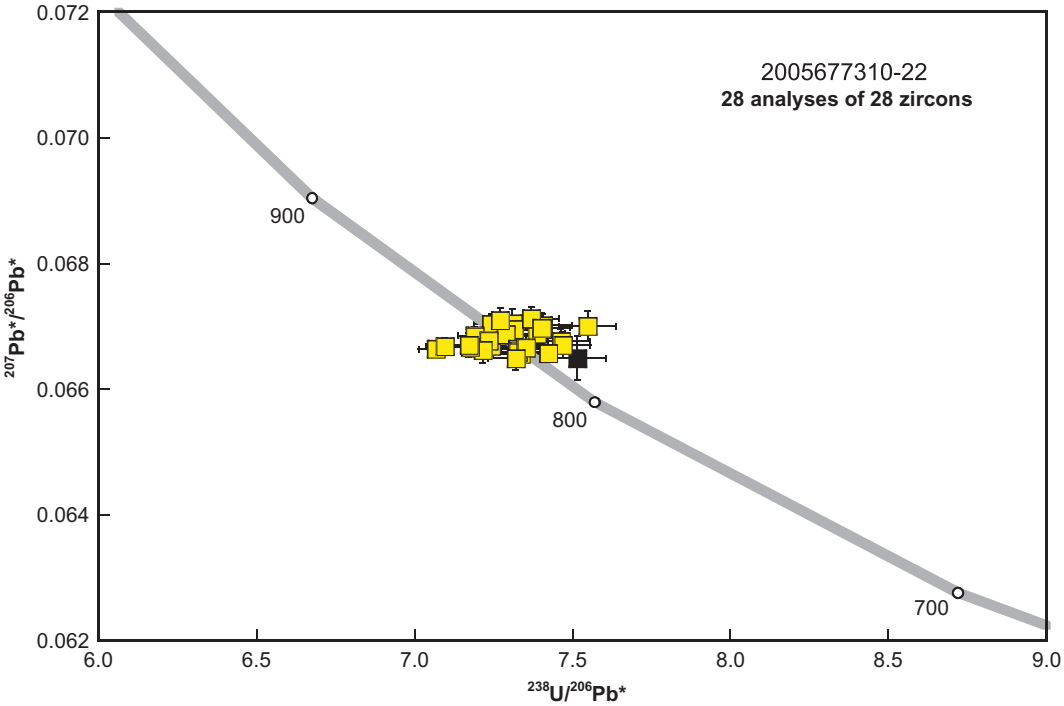

Fig. 5. SHRIMP U–Pb analytical data for sample GA 2005677310-22: leucocratic phase of a gabbroic intrusion, Duke Prospect. Yellow squares indicate Group I (magmatic crystallization); black square indicates Group P (radiogenic-Pb loss). (For interpretation of the references to colour in this figure legend, the reader is referred to the web version of this article.)

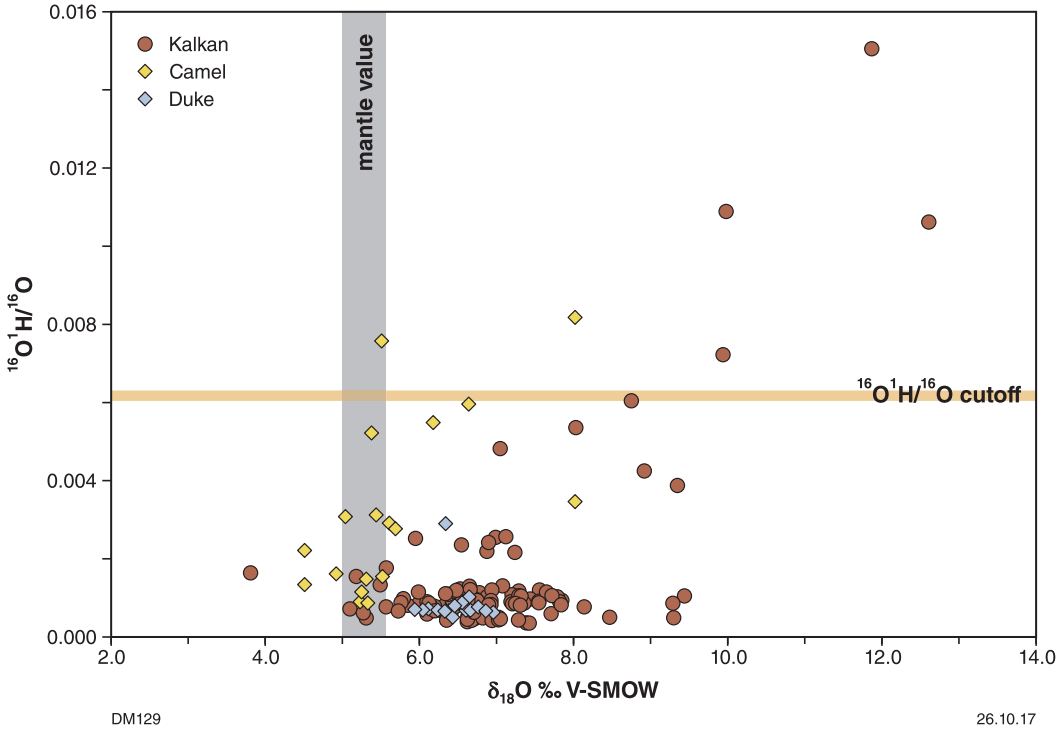

Fig. 6. Plot of $\delta^{18}O$ versus $^{16}O^{1}H/^{16}O$ for the Rudall samples. A $\delta^{18}O$ of 5.3, taken as that of mantle, is marked (Valley, 2003). A relationship between heavy $\delta^{18}O$ (i.e. elevated with respect to mantle value), and elevated $^{16}O^{1}H/^{16}O$, identifies water ingress in metamict crystals. A cutoff of $^{16}O^{1}H/^{16}O \approx 0.006$ is here applied to the data, with those data having a $^{16}O^{1}H/^{16}O$ higher being considered to not reflect primary values, and thus discarded (see text for details).

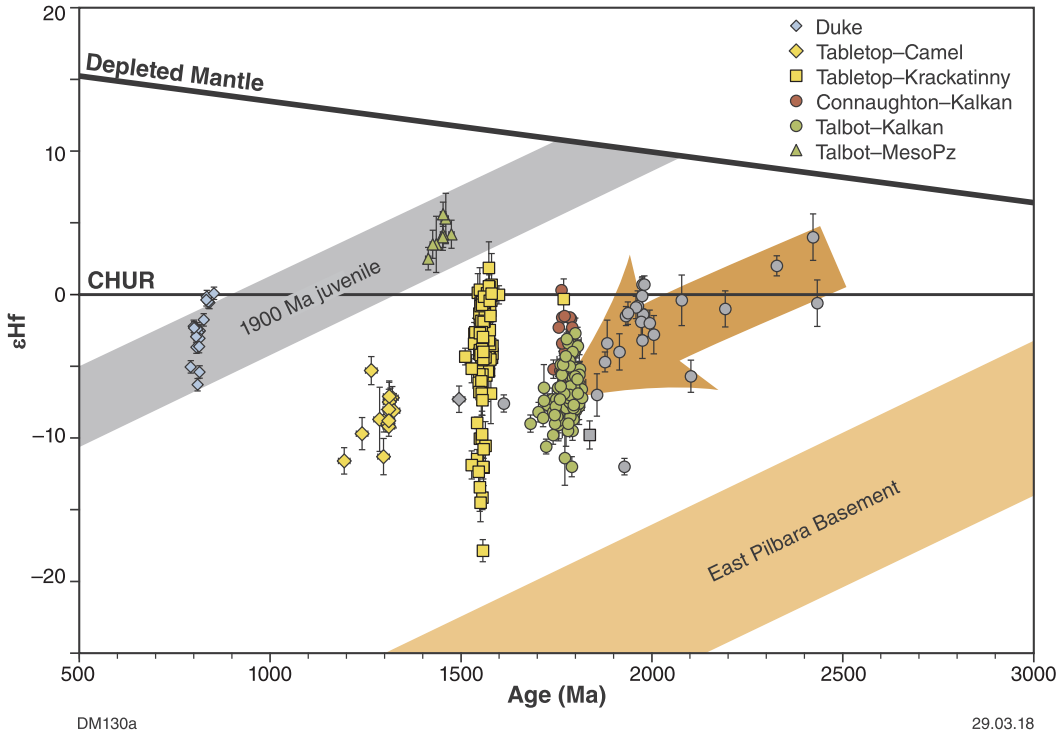

Fig. 7. Hf evolution plot for the Rudall Province samples, coloured by terrane and magmatic suite. Error bars are 2σ. Hf isotope data is that reported here, and from Kirkland et al. (2013b) and GSWA (2016); see Table 1 for details. The orange arrow indicates an interpreted Hf evolution trend for the Kalkan, Krackatinny and Camel magmatic suites. Evolution trends are marked for the Paleoarchean East Pilbara Terrane (data from Gardiner et al. (2017)), and for a ca. 1900 Ma juvenile source interpreted as an input into the Kalkan and Krackatinny Supersuites, and Camel Suite magmatism. (For interpretation of the references to colour in this figure legend, the reader is referred to the web version of this article.)

largely sourced from the melting of heterogeneous crust, or from variable mixing.

Hf evolution diagrams can help discriminate magmatic source and provenance, and allow interpretation of the degree of crustal reworking, or input of foreign material to that crust being reworked. Hf evolution trends are defined by a specific $^{176}Lu/^{177}Hf$ value, which defines a slope in $^{176}Hf/^{177}Hf$ (and thus epsilon) space through production of radiogenic ^{176}Hf with time. Kalkan Supersuite samples from both the Talbot and Connaughton terranes plot within the same domain as defined by magmatic age (largely 1800–1760 Ma), and εHf (Fig. 7). The orange arrow in Fig. 7 indicates an evolution trend that can be drawn from the older analyses of xenocrysts from the Kalkan Supersuite (i.e. those > 1800 Ma). The younger Kalkan rocks, as well as those of the Krackatinny and Camel suites, lie within this trend, suggesting that they may share a common magmatic source, and therefore resolve to similar Meso- to Neoarchean Hf model ages (T_{DM}^2; 2.4–3.4 Ga). The younger Tabletop Terrane magmatic suites — the Krackatinny Supersuite and Camel Suite—also straddle this broad Hf evolution trend, which implies that they incorporated some Kalkan Supersuite material and/or were derived from similar sources to those of the Kalkan Supersuite (Fig. 7). Although broadly similar to the Kalkan Supersuite, the magmatic suites of the Tabletop Terrane, in particular the Krackatinny Supersuite, range to higher εHf values, indicating a larger proportion of juvenile material was incorporated in the source of these magmas.

In contrast to the rocks of the Kalkan and Krackatinny Supersuites and of the Camel Suite, the ca. 1453 Ma granitic boulder from the Talbot Terrane is distinguished on the basis of having (on average) positive εHf. This juvenile Hf signal implies a magmatic source distinct from that of the older magmatic suites, and/or a significantly greater contribution from mantle material during its petrogenesis (represented by the modelled depleted mantle line on Fig. 7). The Hf evolution trend suggests a Paleoproterozoic (ca. 2000–1850 Ma) source for this granitic rock. The juvenile Hf isotopic signature is consistent with its zircon oxygen isotopic composition, which yielded a mantle-like weighted mean $\delta^{18}O$ value of 5.23‰ (Kirkland et al., 2013b).

The Permian Paterson Formation in the area from which the ca. 1453 Ma sample was taken was deposited within a paleovalley system that locally drains from the south-southeast, more regionally from the southeast, and contains granitic boulders up to several metres in diameter (Hickman and Bagas, 1999; Whitaker et al., 2010). Given that the sample does not appear to have been taken from a basement exposure, this raises the question as to whether the sampled boulder was derived from local sources or from outside the Rudall Province, given the sample site is close to the southern margin of the currently exposed province. Although this question is difficult to resolve, it is worth noting that basement rocks immediately to the south and southeast of the Rudall Province remain covered by Neoproterozoic to Permo-Carboniferous sedimentary successions, and are thus unlikely to have been exposed during the Permian. This suggests either a local source for the Mesoproterozoic granitic rock, or transport from well outside the Paterson Orogen. The presence of a similarly aged Mesoproterozoic granitic rock in the Tabletop Terrane (Thevissen, 1991) suggests that a local source may be the more likely possibility. The influence of a ca. 2000–1850 Ma source in the Rudall Province has been previously inferred from whole rock Nd isotopes of the in Kalkan Supersuite, which indicate a component of this age (Kirkland et al., 2013b).

Importantly, the Duke gabbro also yields less evolved εHf than those samples of the Kalkan and Krackatinny supersuites, and the Camel Suite, measuring between −7 and 0 epsilon units. Analyses from the Duke and the ca. 1453 Ma sample plot on what may be a crustal evolution trend that is distinct to the older, Paleo- to Mesoproterozoic Rudall Province Supersuites, implying they are tapping a different, more juvenile, source. Zircons from the Duke gabbro range in $\delta^{18}O$ from 6 to 7‰, which is moderately elevated from the mantle value, and implies some degree of supracrustal input into the magmatic source. These elevated O isotope values contrast with the mantle-like oxygen signature in the ca. 1453 Ma sample, and need to be reconciled with the juvenile Hf isotope signal. One possibility is that the Duke gabbro reflects ca. 830 Ma melting of a ca. 1900 Ma underplate that has seen minor contamination from supracrustal rocks that have experienced near surface processes in which oxygen isotope fractionations are large.

When considering candidate source material as an input into magmatism found across the Rudall Province, attention falls on the Pilbara Craton, which lies immediately to the west of, and possibly underlies, the Rudall Province. The Pilbara Craton has the Paleo to Neoarchean East Pilbara Terrane as its cratonic core. A characterization of an “East Pilbara Basement” Hf isotopic signature can be derived from zircon Hf isotope data measured in Paleo- to Mesoarchean rocks of TTG-affinity from the East Pilbara Terrane, as reported by Gardiner et al. (2017). An evolution trend for this East Pilbara signature is plotted in Fig. 7 (orange). Inspection shows that all the Rudall Province magmatic rocks discussed here lie above this Hf evolution trend, in that they have consistently more juvenile εHf values than if they were solely derived from East Pilbara Basement. This does not exclude East Pilbara Basement as an input into the source of Rudall Province magmatism, specifically the Kalkan, Krackatinny and Camel magmatic suites. However, the Hf isotopes suggest that, if East Pilbara Basement were an input, then it must have been as part of a mix with more juvenile addition. Thus, with a more complete and accurate Pilbara Craton dataset we contrast our interpretation against the findings in Kirkland et al. (2013b), who concluded their Hf data overlapped the most juvenile component of the East Pilbara.

We also conclude there is a possibility of input of ca. 1900 Ma juvenile crust as shown by both the Duke gabbro and ca. 1453 Ma granite samples, and by Nd isotope data from the Kalkan Supersuite (Kirkland et al., 2013b). One likely candidate for this source is “Musgraves-like” crust, i.e. that characterized by rocks outcropping in the Paleo- to Mesoproterozoic Musgrave Province, which lies to the southeast in central Australia. Zircon Hf isotope data from the central Musgrave Province implies a juvenile source at ca. 1900 Ma (Kirkland et al., 2013c). However, the Musgrave Province is ~2000 km away from the Rudall Province, and a more realistic candidate for this ca. 1900 Ma source is a West Australian Craton-girdling Proterozoic ocean. Hence, it may be that oceanic crust of the ca. 1900 Ma Mirning Ocean (and its underplated equivalent), provides an explanation for at least some of the juvenile input into the Rudall Province (Kirkland et al., 2017) (Fig. 7).

Combining zircon oxygen isotope data with the zircon Hf isotope data can further inform on the nature of source, specifically allowing the screening of data for contribution from material that has been exposed to supracrustal processes. Such material will typically exhibit heavier $\delta^{18}O$ than a mantle value of 5.6‰ (Valley, 2003). Plotting εHf versus $\delta^{18}O$ indicates that the Rudall Province data can be split into two broad trends (Fig. 8A). The early magmatism, that of the 1804–1762 Ma Kalkan Supersuite in the Talbot and Connaughton terranes, has an isotopic trend of more mantle like with time (Fig. 8B).

In contrast, granitic rocks from the Tabletop Terrane, both the Krackatinny Supersuite and the Camel Suite, define a trend in εHf–$\delta^{18}O$ space with dominantly mantle-like oxygen isotope values regardless of how evolved the Hf isotopes are (yellow arrow, Fig. 8A). This trend also implies a magmatic source involving the reworking of existing crustal material, but in contrast to that of the Kalkan Supersuite, without any significant incorporation of supracrustal material.

5.1.1. Combined Lu–Hf and Sm–Nd isotopes

For completeness, Fig. 9 shows combined whole-rock εNd and median zircon εHf isotopic data for selected samples from the Rudall where both whole-rock Nd and zircon Hf isotope data are available. The terrestrial array is also marked (Vervoort et al., 2000), and the Rudall data show a scatter around this array.

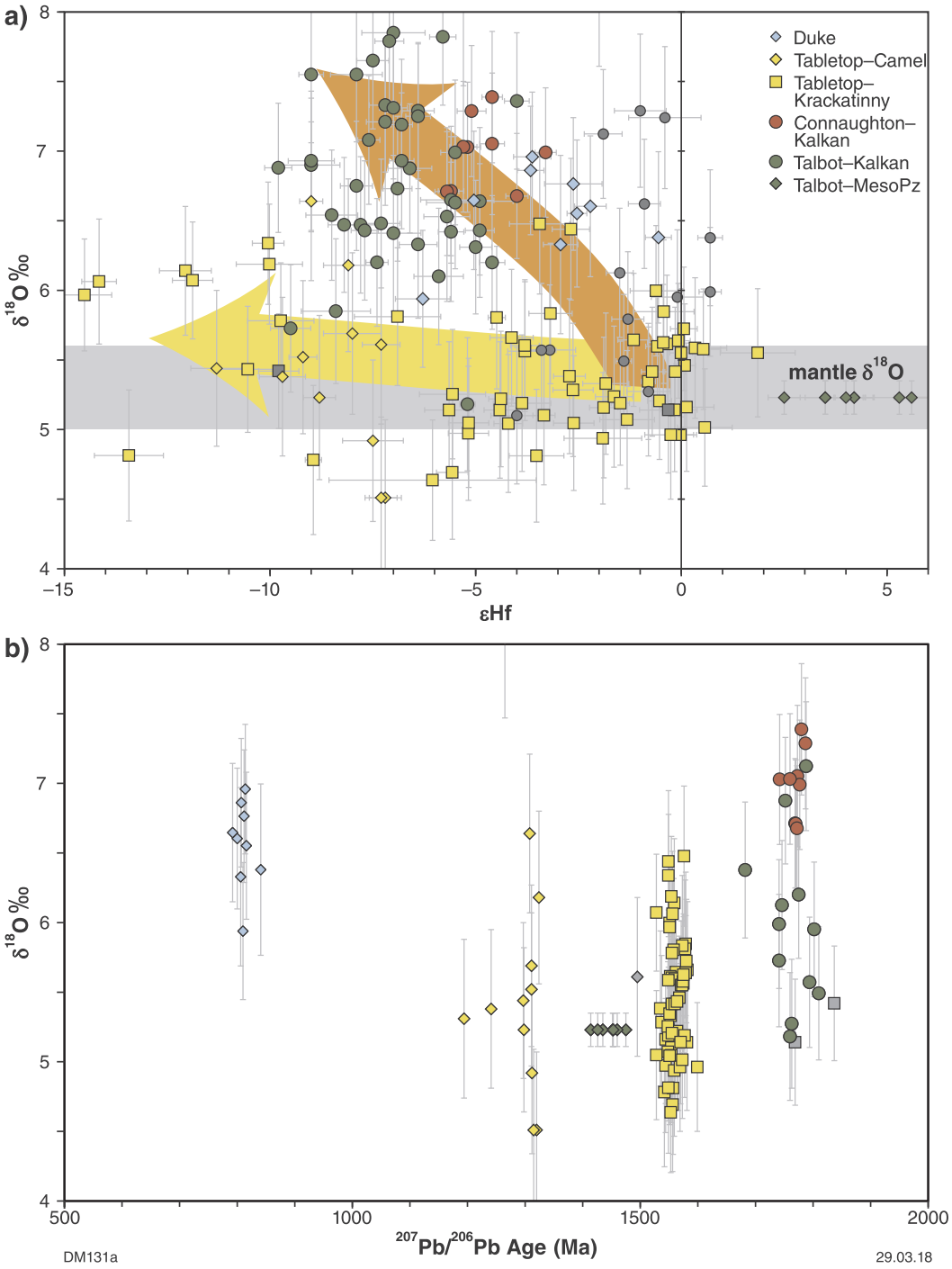

Fig. 8. A. Zircon $\delta^{18}O$ versus εHf for the Rudall samples, annotated by terrane and supersuite. Hf and O isotope data is that reported here, and from Kirkland et al. (2013b) and GSWA (2016); see Table 1 for details. The orange arrow indicates an interpreted Hf evolution trend for the Kalkan Supersuite, and the yellow arrow for the Krackatinny Supersuite and Camel Suite. The grey line refers to a typical mantle oxygen isotope signal of 5.3 ± 0.3‰ (1σ; Valley, 2003). Error bars on individual analyses are 2σ. B. Zircon $\delta^{18}O$ versus age (zircon U-Pb) showing a decrease in oxygen isotope values with time. (For interpretation of the references to colour in this figure legend, the reader is referred to the web version of this article.)

5.2. Geodynamic evolution of the Rudall Province

Fig. 10 shows a time-chart for the major magmatic and orogenic events in the Rudall Province. Here we discuss these magmatic events recorded in the rocks, their implications for a geodynamic model, and specifically how this evidence may record the cratonic assembly of Australia.

5.2.1. Paleoproterozoic (ca. 1800 Ma) events

The 1804–1762 Ma Kalkan Supersuite has previously been interpreted to effectively date moderate- to high-pressure metamorphism in the Rudall Province, and hence the timing of continental collision (Bagas, 2004; Hickman and Bagas, 1999; Smithies and Bagas, 1998). However, more recent studies have suggested that at least some of the Kalkan Supersuite magmatism could have been generated within a locally extensional setting, either caused by rollback of a subducting slab immediately prior to a collision (Betts and Giles, 2006), or by extension

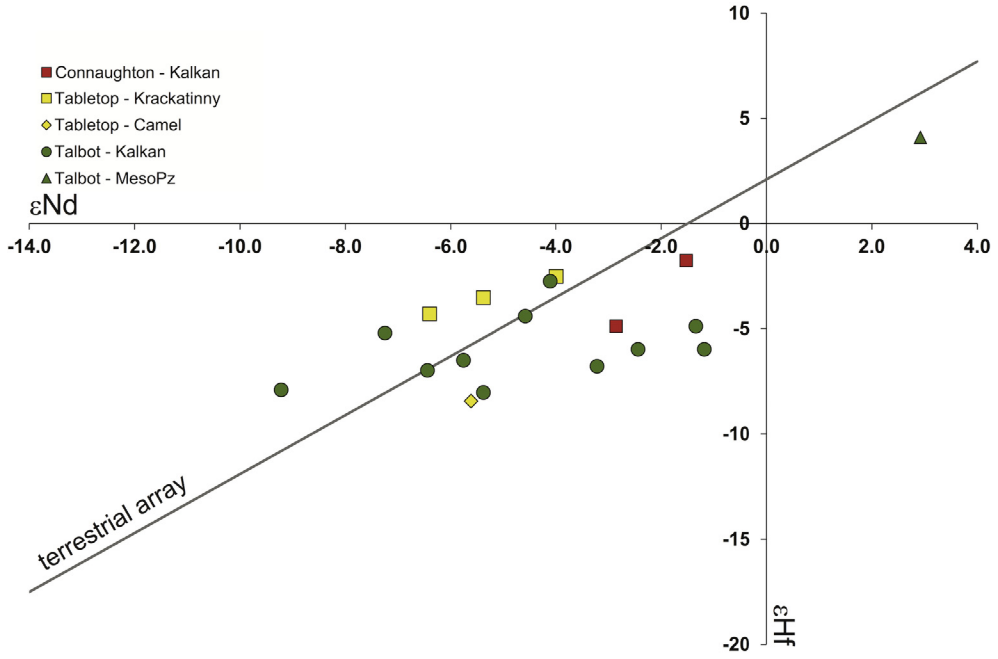

Fig. 9. Zircon εHf versus whole-rock εNd for selected Rudall Province samples. The terrestrial array of Vervoort et al. (2000) is also plotted.

unrelated to a collisional event (Maidment, 2017). Low whole-rock Sr/Y values for the Kalkan Supersuite (Budd et al., 2002; Maidment, 2017) imply melting at depths too shallow for garnet to be a stable phase, which may in turn imply a high geothermal gradient. Such a relatively high geothermal gradient for the generation of Kalkan Supersuite magmatism would perhaps be more consistent with an extensional than compressional setting. Zircons from the Kalkan Supersuite with a trend towards higher $\delta^{18}O$ and more evolved Hf isotopes might reflect higher degrees of crustal reworking during progressive crustal thinning and propagation of heat into higher crustal levels.

Recent studies suggest that the relatively high-pressure metamorphism previously assigned to the Yapungku Orogeny might instead have taken place after the emplacement of the Kalkan Supersuite, possibly as late as ca. 1300 Ma (Anderson, 2015; Maidment, 2017). If this metamorphism is in fact unrelated to Kalkan Supersuite magmatism, it would remove the need to relate the magmatism to structural thickening of the crust during collision. If the Kalkan Supersuite was indeed emplaced in an extensional setting, the broader geodynamic setting of this extension is still unclear. It is possible that this is related to plate margin activity further to the (present day) northeast, but since this area is covered by the Canning Basin, there is little context in which to evaluate the Paleoproterozoic tectonism.

The Bridget Suite is a suite of intrusive igneous rocks comprising lamprophyric syenites to monzodiorites, which forms a narrow north- to northwest-trending belt within the East Pilbara Terrane (Budd et al., 2002; Collins et al., 1988; Hickman, 1978). A sample of monzodiorite from this suite yielded a U–Pb zircon age of 1803 ± 19 Ma, interpreted as the magmatic age (GSWA, 2016), and therefore near-contemporaneous with Kalkan Supersuite magmatism. The Bridget Suite differs geochemically from the Kalkan Supersuite in that it has high Sr/Y, consistent with partial melting at depths greater than ~30–35 km where garnet is stable. The Bridget Suite is also relatively hornblende-rich (Collins et al., 1988), compared to the predominantly biotite-bearing Kalkan Supersuite granitoids. Bridget Suite zircons yielded a range of highly evolved zircon εHf isotope values (−21.2 to −13.7 in the dated monzodiorite; (Kirkland et al., 2013b), consistent with a predominantly East Pilbara Basement source. Bridget Suite rocks have been interpreted as a far-field response to a ca. 1800–1760 Ma collisional Yapungku Orogeny (Bagas, 2005), but a compressional setting is not necessarily implied (Maidment, 2017). The Bridget Suite has been interpreted as having a shoshonitic affinity (Collins et al., 1988), and contains between 63 and 65 wt% SiO_2. It has high K_2O (3.8–4.6 wt%), and very high P_2O_5 (0.28–0.37 wt%) and Ba (621–894 ppm), suggesting a metasomatised lithospheric source component. One possibility is that these hornblende-bearing alkaline rocks reflect low-degree partial melting of previously hydrated sub-continental lithospheric mantle during the early stages of the extensional event that led to the emplacement of the Kalkan Supersuite further to the east.

5.2.2. Early Mesoproterozoic (ca. 1590–1550 Ma) events

Rocks of the Krackatinny Supersuite appear to form three belts in the Tabletop Terrane, each with distinct compositions: (a) an early (1589 ± 5 Ma) sodic and high-Sr/Y suite; (b) a sodic and low-Sr/Y suite; and (c) a younger (1577–1549 Ma) potassic suite (Maidment, 2017); the high and low Sr/Y rocks have tonalite–trondhjemite–granodiorite (TTG)-like affinity, with the high Sr/Y variety implying that these Krackatinny Supersuite rocks, in contrast to the Kalkan Supersuite, were derived from partial melting deep enough to stabilize garnet. However, while TTGs are interpreted to be derived from the melting of hydrated mafic crust (Martin et al., 2005), the evolved Hf and Nd isotope signatures of the Krackatinny Supersuite suggests the mafic source of these rocks was not young oceanic crust (e.g., a subducting slab) or a juvenile mafic underplate emplaced during a rifting event, but was older (Kirkland et al., 2013b). The similarity of Krackatinny Supersuite coupled Hf–Nd isotope signatures to TTGs from the East Pilbara Terrane suggests the mafic source is Pilbara lower crust. Krackatinny Supersuite shows uniformly mantle-like oxygen isotope signals, which suggests a mantle origin for the water required to facilitate melting in this mafic protolith. In contrast, the Kalkan Supersuite has elevated oxygen isotope values, and may be the product of shallower melting (than the Krackatinny) of a stratified crust.

The Krackatinny Supersuite potassic A-type granites have high FeO/(FeO + MgO) ratios, are strongly K-rich (K_2O = 4–6.9 wt%, K_2O/Na_2O = 1–3.3), and have alkali-calcic compositions with enrichments in Nb, Zr, Y and REE (Maidment, 2017). These geochemical signatures are typical of magmas generated within-plate in an extensional setting. The Hf and O isotope signals imply that the Krackatinny Supersuite high Sr/Y rocks formed through deep melting of thickened mafic crust

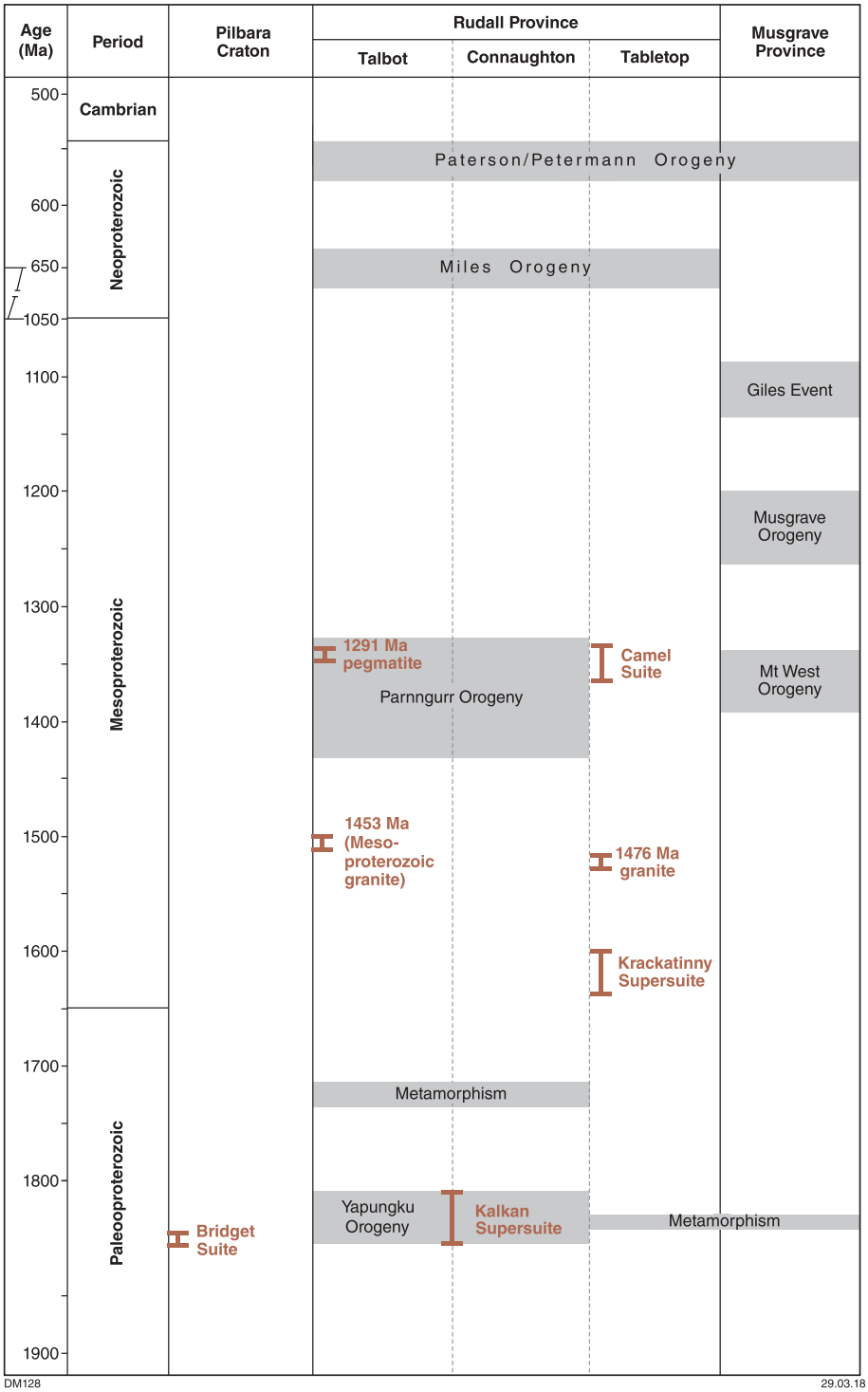

Fig. 10. Geological time/space diagram for major events of the Rudall Province.

of Pilbara affinity, with no requirement for any contribution from subducted crust. Subsequent changes in granite compositions, towards low Sr/Y and then rift-style A-type magmatism, are consistent with deep melting followed by progressive eastwards extension and shallower melting. In summary, the genesis of the Krackatinny ca. 1590–1550 Ma magmatism can be attributed to an extensional setting, developed within crust affected by a previous compressional event. It is possible that this compression was related to metamorphism recorded by limited ca. 1688–1666 Ma dates for metamorphic zircon and monazite (Anderson, 2015; Maidment, 2017), but the nature of this tectonothermal event is currently poorly constrained.

5.2.3. *ca. 1300 Ma events*

Significant high-grade metamorphism in the Talbot and Connaughton terranes has been dated at ca. 1380–1275 Ma (Anderson, 2015; Maidment, 2017), which is here termed the Parnngurr Orogeny. Rocks in the Connaughton Terrane with medium- to high-P peak metamorphic assemblages previously assigned to the ca. 1800–1760 Ma Yapungku Orogeny (Smithies and Bagas, 1997) yielded U–Pb monazite dates of ca. 1341–1295 Ma and a U–Pb zircon date of 1377 ± 26 Ma

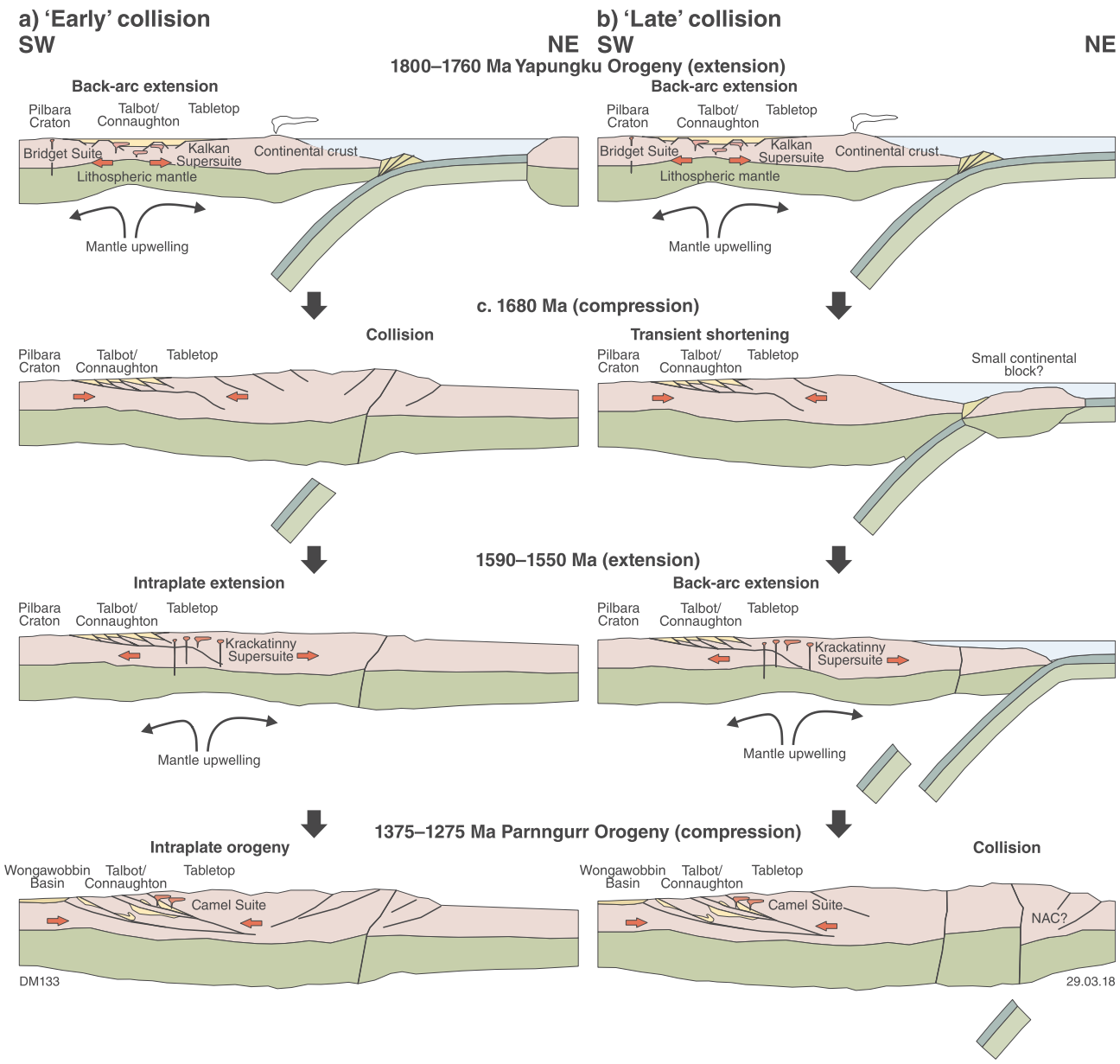

Fig. 11. Schematic cross-sections illustrating two possible scenarios for the tectonic development of the Rudall Province. Both scenarios infer an early extensional setting for magmatism of the 1804–1762 Ma Kalkan Supersuite (Yapungku Orogeny) inboard of a potential plate margin. In both situations a subduction event is inferred at some distance outboard (to the present day east) of the Rudall Province. This subduction may have involved under-plating of ca. 1900 Ma material to allow its subsequent incorporation as a source component in later magmatic events; a process widely inferred on the margin of Archean crust that was reworked in the Proterozoic (Thybo and Artemieva, 2013). A: 'Early' amalgamation between the West Australian Craton and the North Australian Craton, or intervening crustal block. A collision at ca. 1680 Ma resulted in crustal thickening that provided a source for later deep melting during intraplate rifting in the early stages of Krackatinny Supersuite magmatism. Medium- to high-pressure metamorphism and magmatism at ca. 1375–1275 Ma (Parnngurr Orogeny) was a result of intraplate orogeny driven by far-field plate interactions, with magmatism emplaced in the latter stages of tectonism, during extensional relaxation. B: 'Late' amalgamation, involving short-lived compression and crustal thickening at ca. 1680 Ma, possibly as a result of accretion of a small crustal block. Continued convergence between the West and North Australian Cratons resulted in back-arc extension in the eastern Rudall Province at 1590–1550 Ma. Final collision of the West Australian Craton with the North Australian Craton took place at 1375–1275 Ma during the Parnngurr Orogeny (or as a series of prolonged accretional events, as per Anderson (2015).

(Anderson, 2015). Trace element compositions of the metamorphic zircon are consistent with growth in the presence of garnet, and the associated age is considered to reflect the timing of high-P metamorphism. These dates are similar to U–Pb zircon dates of 1334 ± 4 and 1315 ± 21 Ma obtained elsewhere in the Connaughton Terrane (Maidment, 2017). U–Pb dating of metamorphic monazite from rocks with medium pressure assemblages in the Talbot Terrane yielded slightly younger dates of 1283–1275 Ma (Anderson, 2015). No metamorphism of comparable age has yet been dated in the Tabletop Terrane, which suggests that either Mesoproterozoic metamorphism at the currently exposed crustal level was of lower grade (i.e. not recorded by U–Pb chronometers), or that the exposed Tabletop Terrane was not significantly affected by this tectonism, other than by emplacement of granitic rocks of the Camel Suite.

Magmatism of the Camel Suite at ca. 1310–1286 Ma is known from a restricted area near the Camel–Tabletop Fault Zone, and appears to be smaller in volume than either the Krackatinny or Kalkan Supersuites. Camel Suite rocks are K-rich leucogranites with similar geochemical characteristics to the Kalkan Supersuite, and may also have been emplaced in an extensional setting (Maidment, 2017). The limited dating

of this magmatism suggests it was emplaced after the high-P metamorphism in the Connaughton Terrane, and possibly before medium-P metamorphism in the Talbot Terrane to the northwest. Anderson (2015) suggested that the long-lived and possibly diachronous nature of this tectonism across the Rudall Province was a result of the accretion of discrete crustal 'ribbons', previously rifted from the margin of the West Australian Craton. In this model, subduction is envisaged to step outboard during accretion, to eventually place the Rudall Province in a back-arc setting, with final amalgamation with the North Australia Craton along a suture zone further to the northeast at or after 1300–1280 Ma. In this scenario, granitic rocks of the Camel Suite could reflect extension within a back-arc setting following terrane accretion. Alternatively, if the Parnngurr Orogeny was a ca. 1377–1275 Ma intraplate orogenic event, Camel Suite magmatism might reflect extensional collapse or relaxation following the main period of shortening.

5.2.4. Geodynamic model and implications for WAC–NAC assembly

We infer that all terranes of the Rudall Province are para-autochthonous with respect to the Pilbara Craton, extending the conclusion of Kirkland et al. (2013b) who focused on the Kalkan Supersuite. Detrital zircon age components in quartzite from the Tabletop Terrane are consistent with derivation from the Pilbara Craton, and those from quartzite in the Connaughton Terrane are consistent with derivation from sedimentary successions overlying the craton (Maidment, 2017). Given that there is no definitive evidence indicating that in the Kalkan, Krackatinny or Camel suites were emplaced as part of a magmatic arc, all of these are interpreted to have occurred on the margin of the Pilbara Craton, possibly as a result of extension driven by plate boundary processes further to the northeast, which potentially did involve subduction. Differences between the terranes of the Rudall Province, in particular the apparent distribution of the Krackatinny Supersuite, may be the result of partitioning of tectonism and magmatism across major structures such as the Camel–Tabletop Fault Zone, coupled with the effects of younger movements on this structure during the Neoproterozoic Miles and Paterson orogenies. The zircon Hf isotope data of the Kalkan, Krackatinny and Camel suites may be interpreted to indicate an input of ca. 1900 Ma juvenile crustal material in the source of their magmatism; the wider implications for this are discussed below in Section 4.3.

In seeking to constrain the timing of the assembly of the North Australian Craton with the Western Australian Craton, the age of medium- to high-pressure metamorphism in the Rudall Province is an important constraint in that it records significant crustal thickening that might reflect a collisional event. As previously noted, the currently available data suggest that the medium- to high-pressure metamorphism previously assigned to the Yapungku Orogeny in fact took place at 1377–1275 Ma (the Parnngurr Orogeny), allowing for a Mesoproterozoic amalgamation of the West and North Australian Cratons (Anderson, 2015; Maidment, 2017). However, the geodynamic setting of the Parnngurr Orogeny remains unclear, and a more complete understanding of the tectonism in the Rudall Province leading up to this orogenic event is required to assess the timing of craton amalgamation. Complicating this understanding is the possibility that the amalgamation of the West and North Australian Cratons was not a simple collisional event, either reflecting progressive accretion (Anderson, 2015), or involving an intervening crustal block (Frogtech Geoscience, 2017; Maidment and Zhan, 2016). The relatively homogeneous seismic character of the crust beneath the Canning Basin south of the Fitzroy Trough is distinct from that of the Pilbara Craton (West Australian Craton) and the Lamboo Province (North Australian Craton), and is also associated with a slightly deeper Moho. It remains unclear whether this 200–300 km wide zone reflects a Proterozoic accretional belt between the cratons (e.g., Anderson, 2015; Myers et al., 1996; Shaw et al., 1995) or a distinct cratonic block (Frogtech Geoscience, 2017) .

Two potential scenarios for amalgamation are considered in Fig. 11. The first (Fig. 11A) involves an 'early' collision of the West Australian Craton with a continental block to the northeast at ca. 1680 Ma, assuming an extensional setting for 1803–1762 Ma Kalkan Supersuite magmatism. A collision at ca. 1680 Ma would establish a thickened crustal section, which was partially melted during intraplate extension at 1590–1550 Ma. In this scenario, the 1377–1275 Ma Parnngurr Orogeny would reflect an intraplate orogenic event driven by far-field stresses, with the Camel Suite emplaced during crustal relaxation towards the end of this tectonism.

The second scenario (Fig. 11B) assumes a 'late' collision or amalgamation, coincident with ca. 1380–1285 Ma dates for metamorphic zircon and monazite, with much of the 1800–1300 Ma tectonism in the Rudall Province taking place above the extended margin of the Pilbara Craton. In this setting, the thickened crust required to provide a source for the Krackatinny Supersuite was generated during a short-lived episode of compression, possibly a result of accretion of a small continental block at ca. 1680 Ma. One possibility is that the Tabletop Terrane represents this crustal block, having been rifted from the craton margin during 1800–1760 Ma extension and re-amalgamated at ca. 1680 Ma. This scenario would be consistent with the isotopic affinity of the Tabletop Terrane with the West Australian Craton, and also suggests that all the tectonic events that affected the western Rudall Province would be represented in some form in the Tabletop Terrane. However, an apparent lack of evidence for subduction between the Tabletop and Talbot/Connaughton terranes (e.g., arc magmatism between 1760 and 1680 Ma) suggests that subduction, if it occurred at this time, took place outboard of the Tabletop Terrane. In this scenario, final amalgamation with the North Australian Craton, or an intervening crustal block, is then considered to have taken place during the Parnngurr Orogeny.

It is worth noting that neither of these relatively simplistic models adequately explain all the currently available data, and the imperfect understanding of the nature of the various tectonothermal events allows for a range of different interpretations. An apparent paucity of ca. 1680 Ma dates for metamorphism and a lack of known magmatism of this age might argue against an 'early' collisional event at this time. A simple 'late' collisional scenario (i.e. 1377–1275 Ma) is complicated by a lack of either known metamorphism of this age in the Tabletop Terrane, or evidence of pervasive deformation affecting the Krackatinny Supersuite. In this context, a more complex accretion as envisaged by Anderson (2015), or a more distal collision, might be required to account for some of these observations. Significant differential movement of terranes during Neoproterozoic deformation also complicates reconstructions.

In this study, we lean towards a later final amalgamation as it better accommodates: (1) the majority of dates obtained for high-pressure metamorphism; (2) the apparent lack of ca. 1680 Ma magmatism that might reflect a major collisional event; and (3) a simpler geometry that a Mesoproterozoic amalgamation allows for the interpreted zone of convergence between the crustal elements of southern and northern Australia in the Paleo- to Mesoproterozoic. This zone of convergence could potentially have acted as the driver for tectonothermal events recorded along the northeast margin of the West Australian Craton and the southern margin of the North Australian Craton.

5.3. Implications for the assembly of Nuna

The zircon Hf isotope trends show a potential requirement for a source of ca. 1900 Ma juvenile magmatism into the source of the Kalkan, Krackatinny and Camel magmatic suites (Fig. 7, grey trend). This suggestion of a significant input of juvenile material of ca. 1900 Ma age is, however, not unique to the magmatism found within the Rudall Province. Recent zircon Hf isotope studies from other Proterozoic belts across Western Australia and South Australia have also implied a similar aged juvenile source as an input into Proterozoic magmatism.

The Proterozoic Albany-Fraser Orogen lies on the southern and eastern margin of the Yilgarn Craton, and contains a number of autochthonous units (Kirkland et al., 2011). Immediately to the east of the

Albany-Fraser Orogen, lies the Eucla and Bight basins, which are underlain by two basement entities defined through geophysics; the Madura and Coompana Provinces (Spaggiari et al., 2015). A zircon Hf isotope study undertaken on drillcore samples from across these two provinces showed the requirement of a significant input of juvenile oceanic crust at ca. 1950 Ma (Kirkland et al., 2017).

The Musgrave Province in Central Australia lies at the intersection of structural trends resulting from the amalgamation of the North, West and South Australian Cratons. Both whole-rock Nd and zircon Hf isotope data from Musgrave samples imply significant input from a juvenile source at 1950–1900 Ma (Kirkland et al., 2015; Smithies et al., 2011). South of the Musgrave Province, zircon Hf isotope analysis was undertaken on a drillcore sample from the northern Gawler Craton, South Australia. This sample, with a magmatic age of 1914 Ma, showed the requirement for a 1970–1920 Ma juvenile source (Reid et al., 2014).

One pattern that emerges from these disparate studies, is that of the involvement of ca. 1900 Ma oceanic crust within the source of Proterozoic magmatism on the margins of the cratonic entities in modern Australia. This potentially leads to a scenario of older oceanic crust becoming trapped between the mutually assembling North, West and South Australian Cratons. In this, it may resemble the so-called 'extroversion' model of Murphy and Nance (2005), where an interior ocean is consumed on assembly of the supercontinent, in this case Nuna.

6. Conclusions

New zircon U–Pb, O and Lu–Hf isotope data presented herein extend the isotopic dataset from the magmatic rocks across the Rudall Province. This dataset allows further interpretation of the geodynamic setting of the various magmatic suites across the major terranes of the Rudall Province, and places constraints on the potential tectonic evolution of the Rudall Province with respect to the cratonic assembly of Proterozoic Australia.

We favour an extensional rather than compressional setting for the 1804–1762 Ma Kalkan Supersuite, and infer that this magmatism is not linked to moderate to high-P metamorphism in the Rudall Province. The magmatic source of the Kalkan Supersuite is crustal, and is likely to have a significant proportion of East Pilbara Basement. Given the relatively high geothermal gradient which may have been necessary for the genesis of these rocks, a setting of extension is possible, but presumably inboard of any continental margin given the lack of granitic rocks with a clear subduction-related geochemistry.

The ca. 1589–1549 Ma Krackatinny Supersuite is apparently the result of melting of a previously thickened, old, deep crustal source (dominantly comprised of East Pilbara Basement), possibly within an extensional setting, with no definitive evidence of a subduction component. We suggest that ca. 1680 Ma metamorphism might reflect a period of shortening and crustal thickening prior to Krackatinny Supersuite magmatism, but it is unclear if this took place within a collisional setting.

Magmatism at ca. 1450 Ma is volumetrically minor, with juvenile Hf isotopes, suggesting a 1900 Ma juvenile component. The possible glacigenic nature of the granitic rock representing this magmatism makes interpretation difficult, but it possibly has a relatively local provenance and may thus inform on regional sources.

The ca. 1310–1286 Ma Camel Suite represents localised potassic magmatism emplaced during, or towards the end of a prolonged medium- to high-pressure metamorphic event (the Parnngurr Orogeny). The geodynamic setting for its genesis is unclear, but the magmatism is consistent with an extensional setting, possibly orogenic collapse or back-arc extension following accretion. This event may represent the youngest possible timing for the amalgamation of West Australian Craton with the North Australian Craton.

Acknowledgements

NJG acknowledges Curtin University for financial support. DM and RHS publish with the permission of the Executive Director, Geological Survey of Western Australia. SB publishes with the permission of the Chief Executive Officer, Geoscience Australia. The Australian Microscopy & Microanalysis Research Facility, AuScope, the Science and Industry Endowment Fund, and the State Government of Western Australian are acknowledged for contributing to the Ion Probe Facility at the Centre for Microscopy, Characterisation and Analysis at the University of Western Australia. Kevin Cassidy collected the sample from the Duke Prospect used in this study from drillcore kindly provided by Aditya Birla. We thank Pat Bickford and David Mole for their helpful reviews, and Eric Tohver for editorial handling.

Appendix A. Supplementary data

Supplementary data associated with this article can be found, in the online version, at http://dx.doi.org/10.1016/j.precamres.2018.05.003.

References

Aines, R.D., Rossman, G.R., 1986. Relationship between radiation damage and trace water in zircon, quartz and topaz. Am. Mineral. 71, 1186–1193.
Anderson, J., 2015. Metamorphic and Isotopic Characterisation of Proterozoic Belts at the Margins of the North and West Australian Cratons (Ph.D. thesis). University of Adelaide, Adelaide, South Australia, pp. 149.
Bagas, L., 2004. Proterozoic evolution and tectonic setting of the northwest Paterson Orogen, Western Australia. Precambrian Res. 128, 475–496.
Bagas, L., 2005. Geology of the Nullagine 1:100,000 Sheet, 1:100,000 Geological Series Explanatory Notes. Geological Survey of Western Australia, pp. 33.
Bagas, L., Boucher, R., Li, B., Miller, J., Hill, P., Depauw, G., Pascoe, J., Eggers, B., 2014. Paleoproterozoic stratigraphy and gold mineralisation in the Granites-Tanami Orogen, North Australian Craton. Aust. J. Earth Sci. 61, 89–111.
Bagas, L., Lubieniecki, Z., 2001. Copper and Associated Polymetallic Mineralization Along the Camel-Tabletop Fault Zone in the Paterson Orogen, Western Australia, Geological Survey of Western Australia Annual Review 1999–2000. Geological Survey of Western Australia, Perth, Western Australia, pp. 36–41.
Bagas, L., Smithies, R.H., 1998. Geology of the Connaughton 1:100,000 sheet, Geological Series Explanatory Notes. Geological Survey of Western Australia, Perth, pp. 50.
Betts, P.G., Armit, R.J., Stewart, J., Aitken, A.R.A., Ailleres, L., Donchak, P., Hutton, L., Withnall, I., Giles, D., 2016. Australia and Nuna. In: Li, Z.X., Evans, D.A.D., Murphy, J.B. (Eds.), Supercontinent cycles through Earth history. Geological Society of London, pp. 47–81.
Betts, P.G., Giles, D., 2006. The 1800–1100 Ma tectonic evolution of Australia. Precambrian Res. 144, 92–125.
Budd, A.R., Wyborn, L.A.I., Bastrakova, I.V., 2002. The Metallogenic Potential of Australian Proterozoic Granites. Geoscience Australia, Canberra, Record, pp. 152.
Cawood, P.A., Korsch, R.J., 2008. Assembling Australia: Proterozoic building of a continent. Precambrian Res. 166, 1–38.
Collins, W.J., Gray, C.M., Goode, A.D.T., 1988. The Parnell Quartz Monzonite: a Proterozoic zoned pluton in the Archaean Pilbara Block, Western Australia. Aust. J. Earth Sci. 35, 535–547.
Frogtech Geoscience, 2017. Canning Basin SEEBASE Study and GIS Data Package, p. 297.
Gardiner, N.J., Hickman, A.H., Kirkland, C.L., Lu, Y.J., Johnson, T.E., Zhao, J.X., 2017. Processes of Crust Formation in the Early Earth Imaged through Hf isotopes from the East Pilbara Terrane. Precambrian Res. 297, 56–76.
GSWA, 2016. Compilation of Geochronology Information 2016. Geological Survey of Western Australia, Perth.
Hickman, A.H., 1978. Nullagine, Western Australia, 1:250 000 Geological Series Explanatory Notes. Geological Survey of Western Australia, pp. 22.
Hickman, A.H., Bagas, L., 1999. Geological evolution of the Palaeoproterozoic Talbot Terrane and adjacent Meso- and Neoproterozoic successions, Paterson Orogen, Western Australia. Geological Survey of Western Australia, Report, pp. 91.
Huston, D.L., Czarnota, K., Jaireth, S., Williams, N., Maidment, D.W., Cassidy, K.F., Duerden, P., Miggins, D., 2010. Mineral Systems of the Paterson Region. Geoscience Australia, Record, pp. 155–218.
Huston, D.L., Blewett, R.S., Champion, D., 2012. Australia through time: a summary of its tectonic and metallogenic evolution. Episodes 35, 23–43.
Johnson, S.P., Thorne, A.M., Tyler, I.M., Korsch, R.J., Kennett, B.L.N., Cutten, H.N., Goodwin, J., Blay, O.A., Blewett, R.S., Joly, A., Dentith, M.C., Aitken, A.R.A., Holzschuh, J., Salmon, M., Reading, A.M., Heinson, G., Boren, G., Ross, J., Costelloe, R.D., Fomin, T., 2013. Crustal architecture of the Capricorn Orogen, Western Australia and associated metallogeny. Aust. J. Earth Sci. 60, 681–705.
Kirkland, C.L., Spaggiari, C.V., Pawley, M.J., Wingate, M.T.D., Smithies, R.H., Howard, H.M., Tyler, I.M., Belousova, E.A., Poujol, M., 2011. On the edge: U-Pb, Lu–Hf, and Sm–Nd data suggests reworking of the Yilgarn craton margin during formation of the Albany-Fraser Orogen. Precambrian Res. 187, 223–247.
Kirkland, C.L., Johnson, S.P., Smithies, R.H., Hollis, J.A., Wingate, M.T.D., Tyler, I.M.,

Hickman, A.H., Cliff, J.B., Tessalina, S., Belousova, E.A., Murphy, R.C., 2013b. Not-so-suspect terrane: Constraints on the crustal evolution of the Rudall Province. Precambrian Res. 235, 131–149.
Kirkland, C.L., Smithies, R.H., Woodhouse, A.J., Howard, H.M., Wingate, M.T.D., Belousova, E.A., Cliff, J.B., Murphy, R.C., Spaggiari, C.V., 2013c. Constraints and deception in the isotopic record; the crustal evolution of the west Musgrave Province, central Australia. Gondwana Res. 23, 759–781.
Kirkland, C.L., Johnson, S.P., Smithies, R.H., Hollis, J.A., Wingate, M.T.D., Tyler, I.M., Hickman, A.H., Cliff, J.B., Belousova, E., Murphy, R.C., Tessalina, S., 2013a. The crustal evolution of the Rudall Province from an isotopic perspective. Geological Survey of Western Australia, pp. 30 Report 122.
Kirkland, C.L., Smithies, R.H., Spaggiari, C.V., 2015. Foreign contemporaries – unravelling disparate isotopic signatures from Mesoproterozoic Central and Western Australia. Precambrian Res. 265, 218–231.
Kirkland, C.L., Smithies, R.H., Spaggiari, C.V., Wingate, M.T.D., Quentin de Gromard, R., Clark, C., Gardiner, N.J., Belousova, E.A., 2017. Proterozoic crustal evolution of the Eucla basement, Australia: Implications for destruction of oceanic crust during emergence of Nuna. Lithos 278–281, 427–444.
Ludwig, K.R., 2004. User's Manual for Isoplot, 3.16: A Geochronological Toolkit for Microsoft Excel. Berkeley Geochronology Center Special Publication, Ridge Road, Berkeley CA, USA.
Maidment, D.W., 2017. Geochronology of the Rudall Province, Western Australia: implications for the amalgamation of the West and North Australian Cratons. Geological Survey of Western Australia, pp. 95 Report 161.
Maidment, D.W., Huston, D.L., Maas, R., Czarnota, K., Neumann, N., McIntyre, A., Bagas, L., 2008. The Nifty–Kintyre–Duke Cu–U–Pb– Zn Mineralizing Events: Links to the Evolution of the Yeneena Basin, Northwest Paterson Orogen, GSWA 2008 Extended Abstracts: Promoting the Prospectivity of Western Australia; Record 2008/2. Geological Survey of Western Australia, pp. 27–29.
Maidment, D., Zhan, Y., 2016. Canning coastal seismic survey preliminary basement interpretation (poster). Geological Survey of Western Australia, GSWA Open Day. Geological Survey of Western Australia, Fremantle, Western Australia.
Martin, H., Smithies, R.H., Rapp, R., Moyen, J.F., Champion, D., 2005. An overview of adakite, tonalite–trondhjemite–granodiorite (TTG), and sanukitoid: relationships and some implications for crustal evolution. Lithos 79, 1–24.
Murphy, J.B., Nance, R.D., 2005. Do supercontinents turn inside-in or inside-out? Int. Geol. Rev. 47, 591–619.
Myers, J.S., Shaw, R.D., Tyler, I.M., 1996. Tectonic evolution of Proterozoic Australia. Tectonics 15, 1431–1446.
Nifty, B., 2008. Combined Report C155/2002 Tenements M271 SA, E45/2150-57, E45/2280, E45/2392 and E45/2415 for the period 6th September 2007 to 5th September 2008. Birla Nifty Pty Ltd: Geological Survey of Western Australia Statutory mineral exploration report.
Occhipinti, S.A., Sheppard, S., Passchier, C., Tyler, I.M., Nelson, D.R., 2004. Palaeoproterozoic crustal accretion and collision in the southern Capricorn Orogen: the Glenburgh Orogeny. Precambrian Res. 128, 237–255.
Pidgeon, R.T., Nemchin, A., Cliff, J.B., 2013. Interaction of weathering solutions with oxygen and U-Pb isotopic systems of radiation-damaged zircon from an Archean granite, Darling Range Batholith, Western Australia. Contrib. Mineral. Petrol. 166, 511–523.
Plumb, K.A., 1979. The tectonic evolution of Australia. Earth Sci. Rev. 14, 205–249.
Reid, A.J., Jagodzinski, E.A., Armit, R.J., Dutch, R.A., Kirkland, C.L., Betts, P.G., Schaefer, B.F., 2014. U-Pb and Hf isotopic evidence for Neoarchean and Paleoproterozoic basement in the buried northern Gawler Craton, South Australia. Precambrian Res. 250, 127–142.
Shaw, R.D., Wellman, P., Gunn, P., Whitaker, A.J., Tarlowski, C., Morse, M.P., 1995. Australian crustal elements map: a geophysical model for the tectonic framework of the continent. AGSO Res. Newslett. 23, 1–3.
Sheppard, S., Bodorkos, S., Johnson, S.P., Wingate, M.T.D., Kirkland, C.L., 2010. The Paleoproterozoic Capricorn Orogeny: intracontinental reworking not continent–continent collision. Geological Survey of Western Australia Report, Perth, pp. 33.
Smithies, R.H., Bagas, L., 1998. The Tabletop Terrane of the Proterozoic Rudall Complex: preliminary notes on the geology, granitoid geochemistry and tectonic implications. Geological Survey of Western Australia Annual Review 1996–97, pp. 89–94.
Smithies, R.H., Bagas, L., 1997. High pressure amphibolite-granulite facies metamorphism in the Paleoproterozoic Rudall Complex, central Western Australia. Precambrian Res. 83, 243–265.
Smithies, R.H., Howard, H.M., Evins, P.M., Kirkland, C.L., Kelsey, D.E., Hand, M., Wingate, M.T.D., Collins, A.S., Belousova, E., 2011. High-temperature granite magmatism, crust-mantle interaction and the Mesoproterozoic intracontinental evolution of the Musgrave Province, Central Australia. J. Petrol. 52, 931–958.
Spaggiari, C.V., Kirkland, C.L., Smithies, R.H., Wingate, M.T.D., Belousova, E., 2015. Transformation of an Archean craton margin during Proterozoic basin formation and magmatism: the Albany-Fraser Orogen, Western Australia. Precambrian Res. 266, 440–466.
Stacey, J.S., Kramers, J.D., 1975. Approximation of terrestrial lead isotope evolution by a two-stage model. Earth Planet. Sci. Lett. 26, 207–221.
Steiger, R.H., Jager, E., 1977. Subcomission on geochronology: convention on the use of decay constants in geo- and cosmochemistry. Earth Planet. Sci. Lett. 36, 359–362.
Thevissen, J., 1991. 1990–91 Annual Report, Karara Well Project, E45/841, Rudall River area, W.A., Geological Survey of Western Australia, Statutory mineral exploration report. PNC Exploration (Australia) Pty Ltd.
Thybo, H., Artemieva, I.M., 2013. Moho and magmatic underplating in continental lithosphere. Tectonophysics 609, 605–619.
Valley, J., 2003. Oxygen isotopes in zircon. Rev. Mineral. Geochem. 53, 343–385.
Van Kranendonk, M.J., Kirkland, C.L., Cliff, J., 2015. Oxygen isotopes in Pilbara Craton zircons support a global increase in crustal recycling at 3.2Ga. Lithos 228–229, 90–98.
Vervoort, J.D., Patchett, P.J., Albarède, F., Blichert-Toft, J., Rudnick, R.L., Downes, H., 2000. Hf-Nd isotopic evolution of the lower crust. Earth Planet. Sci. Lett. 181, 115–129.
Whitaker, A.J., Roach, I.C., Liu, S.F., Wilford, J.R., 2010. Geology, in: Roach, I.C. (Ed.), Geological and Energy Implications of the Paterson Airborne Electromagnetic (AEM) Survey, Western Australia, pp. 49–86.